



Cite this: DOI: 10.1039/d5bm01885d

# Mechanobiological regulation of endothelial vascularization after myocardial infarction: matrix mechanics, hydrogel strategies and applications

Yanzhe Qian<sup>a,b</sup> and Yuan Yao  <sup>\*a,b,c</sup>

Myocardial infarction (MI) triggers a wound-healing cascade that restores structural integrity but reshapes the cardiac mechanical microenvironment. The transition from compliant, healthy myocardium to stiff, fibrotic scar tissue creates biomechanical barriers that can impede neovascularization and contribute to heart failure progression. These biomechanical cues regulate endothelial fate decisions, including migration, proliferation, branching, and lumen formation, and thus influence neovascularization and perfusion recovery. This review addresses the mechanobiological principles governing endothelial cell behaviours and their translation into biomaterials-based strategies for cardiac regeneration or disease modelling. We first characterize the pathological remodelling cascade following MI, detailing the compositional and architectural shifts from healthy to infarcted myocardium. We then summarize how mechanical properties such as stiffness, viscoelastic stress relaxation, porosity, anisotropy, and degradability function as active regulators of endothelial activation, migration, junctional stability, and morphogenesis and ultimately angiogenesis in two- and three-dimensional environments. Subsequently, we evaluate various hydrogel platforms and tuning strategies, outlining how specific base composition, crosslinking chemistry, and network architecture are leveraged to modulate mechanical cues. Building on these mechanistic insights, we review hydrogel-based *in vitro* vascular models that emulate aspects of the post-infarct myocardium, including self-assembled endothelial–stromal networks, macroporous and granular scaffolds, organ-on-chip platforms with perfused microvessels, and 3D bioprinting approaches. Finally, we discuss limitations in decoupling mechanical from biochemical and architectural cues and in assessing vascular integration, perfusion, and functional outcomes *in vivo*. Altogether, this review highlights design principles for selecting and tuning matrix mechanics in biomaterial platforms aimed at supporting endothelial-driven revascularization of infarcted myocardium.

Received 23rd December 2025,  
Accepted 28th April 2026

DOI: 10.1039/d5bm01885d

rsc.li/biomaterials-science

## 1. Introduction

Myocardial infarction (MI) remains one of the leading causes of mortality worldwide.<sup>1</sup> It occurs when coronary occlusion deprives a region of the myocardium of oxygen, causing massive cardiomyocyte death and triggering a wound-healing cascade. The injured cardiac tissue undergoes pathological remodelling characterized by inflammation, fibrosis, and scar formation.<sup>2</sup> While this process restores structural integrity, it results in a stiff, collagen-rich scar with compromised contractility and inadequate vascularization.<sup>3</sup> Nascent blood vessel

networks that form during healing are often disorganized and insufficient to fully reperfuse the tissue, perpetuating hypoxia.<sup>4</sup> This accelerates adverse ventricular remodelling and predisposes patients to heart failure. Thus, restoring a patterned, perfusable blood supply through neovascularization is essential for functional cardiac recovery. However, efforts to stimulate neovascularization have had limited clinical success, in part due to an incomplete understanding of how the biophysical microenvironment post MI regulates endothelial cell (EC) behaviours.

ECs orchestrate new vessel formation through activation, migration, and morphogenesis into stabilized tubes.<sup>5,6</sup> It has become increasingly evident that extracellular matrix (ECM) mechanics plays instructive roles in vascular morphogenesis, in coordination with angiogenic growth factors, such as vascular endothelial growth factor A (VEGF-A) and fibroblast growth factor 2 (FGF-2).<sup>7,8</sup> Post-MI, the ECM undergoes major mechanical alterations including increased stiffness, altered

<sup>a</sup>Department of Mechanical Engineering, University of British Columbia, Vancouver, BC V6T 1Z4, Canada. E-mail: yuan.yao@ubc.ca

<sup>b</sup>Centre for Heart Lung Innovation, University of British Columbia, Vancouver, BC V6Z 1Y6, Canada

<sup>c</sup>Department of Medicine, University of British Columbia, Vancouver, BC V6T 1Z8, Canada



viscoelasticity, and structural reorganization. ECs sense these changes through integrins and other mechanotransducers. This aberrant mechanosensing can shift endothelial behaviour toward a pro-inflammatory, hyperpermeable, and EndMT-prone state. These responses impair vascular stability, adhesion, and migration, promote maladaptive signalling and fibrosis, and ultimately hinder functional revascularization.<sup>8–10</sup> The growing recognition of the interplay between ECM mechanics and angiogenesis has spurred the development of biomaterials-based platforms to model and manipulate the post-MI environment.<sup>11–13</sup> Hydrogels and engineered matrices with tunable mechanical properties are effective tools in dissecting EC mechanobiology and guiding therapeutic vascularization. These materials have also enabled the development of increasingly sophisticated *in vitro* platforms that capture key aspects of the post-MI microenvironment. Such systems have provided critical mechanistic insight into angiogenic regulation and offer translational opportunities for designing therapies that modulate matrix mechanics to enhance microvascular regeneration.

Angiogenesis following MI and the development of cardiac biomaterials have each emerged as major research directions aimed at restoring perfusion and cardiac function, yet a mechanobiological perspective that systematically connects the evolving post-MI ECM environment with endothelial vascularization and hydrogel design remains underexplored. In this review, we will integrate a mechanobiological analysis of how mechanical parameters regulate endothelial vascularization while translating these mechanistic insights into rational hydrogel design principles for cardiac repair. We first outline the pathological remodelling of cardiac tissues post-MI, with a focus on ECM mechanics and review how these mechanical properties impact EC fate and vascular morphogenesis. We then discuss strategies to tune these mechanical properties in hydrogel platforms, and finally evaluate advanced *in vitro* models designed to probe and promote revascularization in mechanically defined environments. Altogether, we aim to provide a cohesive framework for understanding and leveraging matrix mechanics in cardiac revascularization and to identify opportunities for developing next-generation hydrogel biomaterial-based strategies to restore microvascular function in ischemic diseases. By clarifying how material properties regulate endothelial responses post-MI, this framework may help inform the design of targeted biomaterials that support functional revascularization within the fibrotic post-MI microenvironment.

## 2. Vascular response to pathological matrix remodelling

### 2.1 Vascular remodelling following myocardial infarction

To develop hydrogel-based strategies that restore endothelial vascularization after MI, it is first necessary to understand the pathological mechanical environment that ECs encounter in the remodelling myocardium. The vascular response to MI is

fundamentally shaped not only by biochemical signalling but also by the rapidly evolving mechanical environment of the infarct. As the ECM transitions from a soft provisional matrix to a stiff fibrotic scar, ECs are exposed to progressively altered mechanical cues that compromise vascular repair. This section describes the post-MI changes in microvascular architecture and ECM composition and mechanics that together establish the pathological mechanical context in which endothelial mechanobiological regulation operates.

After a myocardial infarction, the coronary microvasculature undergoes a dynamic but incomplete remodelling. The process begins with transient angiogenic proliferation, followed by pruning and structural maturation of vessels.<sup>14,15</sup> In the infarcted region, capillary density drops precipitously immediately after MI due to ischemic necrosis, and although angiogenesis over the first 1–2 weeks repopulates the infarct with new capillaries, their density remains below that of normal myocardium. Although in large-animal models like pigs and dogs, capillary density in ischemic myocardium can transiently approach or exceed normal levels during peak angiogenesis (*e.g.* dogs ~2960 capillaries per mm<sup>2</sup> at ~1 week),<sup>16–18</sup> many of these microvessels regress as tissue remodels into a fibrous scar. Chronic human infarct scars consequently show capillary densities 40–60% lower than healthy heart tissue.<sup>18–20</sup> Meanwhile, surviving myocardium remote from the infarct often experiences microvascular rarefaction as well, and is associated with impaired pro-angiogenic signalling, such as higher VEGFR-1/VEGF-A ratios and elevated endostatin and hepatocyte growth factor (HGF). Ultimately, post-MI patients exhibit approximately half the capillary density in remote areas compared to non-infarcted heart.<sup>21</sup>

In tandem with quantitative changes, vessel morphology and network architecture change markedly. Neovessels formed within the infarct often exhibit an irregular diameter and lack perivascular support. Over weeks, a subset of these microvessels shows increased perivascular smooth muscle coverage and more arteriole-like morphology. However, this results in the regression of smaller branches, leading to a sparser and coarser microvascular network. Studies have documented a shift toward larger average vessel diameter in healing infarcts, accompanied by a decrease in the total number of microvascular segments.<sup>22</sup> Fractal analysis further reveals reduced branching complexity and connectivity and increased spatial heterogeneity.<sup>22</sup> By the chronic remodelling phase, months post-MI, the infarct microvascular network is relatively sparse, with fewer capillaries and a relatively preserved population of small arteries/arterioles.<sup>22,23</sup> The compromised microvasculature implies longer diffusion distances and worse oxygenation within the scar, while microvascular rarefaction in the remote myocardium is associated with an imbalance of angiogenic factors and progressive ventricular dysfunction. This vascular remodelling occurs in parallel with substantial alteration in ECM structure and composition.<sup>24,25</sup> Importantly, these vascular dynamics and ECM stiffening unfold within an infarct matrix whose mechanics change rapidly during healing. ECs actively interpret this stiffening *via* various mechanosensors,



resulting in limited vasculature sprouting and microvessel instability. Altogether, this mechanobiological coupling between scar maturation and endothelial fate provides a unifying framework for the capillary pruning described above and motivates biomaterial strategies that restore a permissive mechanical environment for reperfusion.

## 2.2 Extracellular matrix remodelling following myocardial infarction

The ECM is a dynamic and instructive microenvironment that regulates cell behaviour through biochemical signalling and biophysical cues. The healthy myocardial ECM maintains the tissue architecture and transmits mechanical forces that preserve endothelial functions. For example, cardiac ECM keeps cardiomyocytes mechanically aligned for efficient force transmission, preserves endothelial barrier stability *via* laminin/collagen IV–integrin contacts, and provides a scaffold that guides endothelial sprouting and lumen formation during vascular morphogenesis.<sup>26,27</sup>

The cardiac ECM is composed primarily of fibrillar collagens (type I and III), elastin, proteoglycans (PG), glycosaminoglycans (GAGs), and glycoproteins such as fibronectin and laminin.<sup>28</sup> Under physiological conditions, collagen I constitutes approximately 85% of the cardiac fibrillar collagen, providing tensile strength *via* dense bundles in the epimysium and perimysium.<sup>29,30</sup> Collagen III (11% of the cardiac collagen) coexists with type I within perimysial and pericellular endomysial collagen struts,<sup>31</sup> and forms thinner, more elastic fibres that confer resilience and elastic recoil.<sup>32</sup> Elastin in coronary vessels and the pericardium provides elasticity and aids elastic recoil during diastole<sup>33</sup> and intact vascular elastin also creates a quiescent, anti-inflammatory niche for ECs to maintain shear-dependent nitric-oxide signalling and barrier function.<sup>34</sup> Proteoglycans, such as decorin and biglycan, organize collagen

fibres, keep the tissue hydrated, and contribute to overall mechanical stability. Specifically, decorin can sequester TGF- $\beta$ -driven fibrosis, whereas biglycan is required for normal collagen fibril assembly and mechanical strength in the healing myocardium.<sup>35,36</sup> Scaffolding is further supported by glycoproteins, such as fibronectin, which provides a provisional ECM for endothelial adhesion and migration during new-vessel formation, and laminin-rich basement membranes envelop cardiomyocytes and vessels to stabilise cell contacts and maintain barrier integrity.<sup>37–39</sup> Finally, the heart contains a small amount of hyaluronic acid (HA)-rich glycosaminoglycan (<0.5% of dry weight in porcine heart), which in healthy hearts functions to bind water and cytokines, and regulates cell mechanosensing *via* endothelial glycocalyx. After MI, activated fibroblasts secrete high-molecular-weight HA which accumulates within the ECM in the infarct zone in similar abundance to collagen.<sup>40,41</sup> The HA forms a hydrated, HA-rich scar that impairs macrophage phagocytic function, dampens angiogenesis, and alters microvascular barrier properties.<sup>40</sup> Comparatively, the ECM remodels after MI and is eventually replaced by a higher concentration of stiff, cross-linked type I collagen-rich scar,<sup>42</sup> as summarized in Table 1. The scar tissue and adjacent remote myocardium feature elevated stiffness (2–4 times increase).<sup>31,43</sup> This is also supported by cardiac magnetic resonance elastography in porcine MI, where infarct-region stiffness exceeds remote myocardium at subacute stages (14 days: 4.6 kPa infarct *vs.* 3.0 kPa remote), and by *ex vivo* tensile testing showing a substantially higher modulus in infarct tissue (650  $\pm$  80 kPa infarcted *vs.* 110  $\pm$  20 kPa remote).<sup>44</sup> In parallel with this mechanical stiffening, MI drives a massive expansion of the extracellular space. The porcine infarct extracellular volume fraction (ECV) increases from 25–26% pre-MI to 48% by day 10 and 53% by day 21, while remote tissue remains near baseline. Notably, infarct

**Table 1** ECM composition and mechanical properties of healthy myocardium *versus* post-myocardial infarction (MI) scar tissue

ECM component	Healthy myocardium composition	Post-MI infarct scar composition
Collagen I	80–85% of total collagen; organized into a hierarchical fibre network <sup>29,30</sup>	Dominant component (>90% of collagen). Forms thick, highly cross-linked fibre bundles <sup>52–55</sup>
Collagen III	10–15% of total collagen; primarily in the endomysium <sup>31</sup>	Initially deposited in the provisional matrix; constitutes a lower proportion (5–10%) of total collagen in the mature scar <sup>56</sup>
Total collagen	~49 mg per g dry weight in normal human LV myocardium, epicardium 5.1 $\pm$ 0.4 in a canine model	95.3 $\pm$ 9.7 mg per g dry weight in dilated cardiomyopathy hearts; epicardium: 51.3 $\pm$ 5.9 mg g <sup>-1</sup> in canine models <sup>29,57</sup>
Elastin	Low in myocardium <sup>58</sup>	Largely degraded and fragmented following MI, contributing to reduced tissue compliance and increased stiffness <sup>57</sup>
Fibronectin	Low levels; primarily the cellular isoform <sup>37–39,59–61</sup>	Transiently upregulated in the early provisional matrix; levels return to baseline in the mature scar <sup>62–64</sup>
Laminin and collagen IV	In basement membranes (BMs) of myocytes and vessels <sup>65–69</sup>	Re-deposited in new BMs: around new capillaries and border zone myocytes, but scar core has little as myocytes are gone <sup>65–69</sup>
Proteoglycans (decorin, biglycan)	Low levels; functions to regulate collagen fibres and distribute mechanical load <sup>35,36</sup>	Upregulated during granulation tissue formation; incorporated into the mature scar to modulate collagen fibre organization <sup>35,36</sup>
GAGs (HA, versican, etc.)	Baseline low HA, PG-bound GAGs present <sup>65–69</sup>	Early surges of HA and versican accumulate in early infarct to form matrix aiding cell infiltration; later removed as collagen matrix matures <sup>65–69</sup>
Matricellular proteins	Very low in healthy adult heart <sup>70</sup>	Dramatically spike early in infarct border zone modulating repair; largely disappear in chronic scar <sup>70</sup>
Mechanical properties	Compliant and anisotropic ( <i>e.g.</i> , passive stiffness of ~10–15 kPa in rat LV). <sup>71</sup>	5–10 times stiffer, less compliant; early scar $\approx$ 50 kPa (~2 weeks) and 0.5–1 MPa in mature scar <sup>31,71</sup>



ECV correlates positively with tissue stiffness, and diffusion MRI indicates that these microstructural shifts impose severe transport constraints, altering the mean free pathway for cells and soluble signals.<sup>45</sup> Concurrently, this deteriorating physical and transport environment restricts the microvascular architecture. In a pig MI model with 3D microvascular reconstruction, infarcted myocardium showed decreases by day 7 in microvascular density-like measures such as vascular length density  $1.65 \times 10^{-3} \mu\text{m} \mu\text{m}^{-3}$  at infarct day 7 vs.  $3.51 \times 10^{-3} \mu\text{m} \mu\text{m}^{-3}$  in basal tissue alongside declines in capillary volume fraction.<sup>46</sup> This stiffening precipitates diastolic dysfunction, compromises ventricular relaxation, and drives adverse remodelling marked by chamber dilation, wall thinning, and geometric distortion. It also creates a microenvironment that is less permissive for vascularization and more prone to arrhythmogenesis.<sup>47–51</sup>

The cardiac ECM remodels over three main phases: inflammatory phase, proliferative phase, and maturation phase. The inflammation phase begins within hours after MI and lasts a few days. Ischemic injury causes cardiomyocyte necrosis and triggers an acute inflammatory response. Matrix degradation is an early event as ischemia-activated matrix metalloproteinases (MMPs) contribute to the cleavage of pre-existing myocardial collagens and other ECM proteins,<sup>72,73</sup> releasing elastin and collagen-derived fragments that recruit and activate neutrophils.<sup>65</sup> These fragments have divergent vascular effects. Collagen-IV fragments such as tumstatin decrease endothelial proliferation and migration, thus decreasing angiogenesis.<sup>66,74</sup> In contrast, elastin peptides can promote neovascularization and angiogenic endothelial responses. Thus, their overall influence on angiogenesis hinges on the balance of specific fragments present.<sup>65</sup>

The inflammation responses are further amplified by laminin fragments and low-molecular-weight HA.<sup>65–69</sup> As macrophages clear necrotic debris, activated cardiac fibroblasts (myofibroblasts) deposit a provisional loose, thin, type III collagen-rich ECM.<sup>43,49,75,76</sup> In this proliferative phase, the provisional fibrin-based matrix is progressively replaced by a cell-derived matrix rich in fibronectin and increasing amounts of hyaluronan. Concurrent plasmin/MMP activity contributes to ongoing ECM remodelling; both deficient and excessive proteolysis have been shown to impair infarct healing, indicating that a balanced relationship between matrix synthesis and degradation is required.<sup>26,52</sup> This phase is also characterised by intense reparative angiogenesis with ECM composition and structure providing a permissive scaffold for orderly capillary sprouting and stabilisation.<sup>77</sup> Fibronectin provides adhesive substrate for endothelial  $\alpha 5 \beta 1$ -integrins,<sup>62,63</sup> while fibroblast-derived hyaluronan accumulates within the extracellular matrix, contributing to the formation of a hydrated matrix.<sup>40,41</sup> The maturation phase of infarct healing occurs in the subsequent weeks and months, as the granulation tissue gradually transitions into a permanent scar. This phase is characterized by increased collagen I deposition and ECM cross-linking, and a decline in elastin, cellularity and vascularity.<sup>52–55</sup> As collagen accumulates and crosslinks, matrix stiffness increases dra-

stically. These changes are correlated with suppressed angiogenesis, reduced myocardial contractility, and thus limited functional recovery.

This dramatic compositional shift characterized by collagen I dominance, elastin depletion, and reduced proteoglycans/GAGs fundamentally alters the infarct scar's mechanical landscape, increasing tissue stiffness and altering the viscoelastic properties of the infarct matrix. The resulting changes in ECM mechanical properties are not merely a passive structural outcome, but also potent biomechanical regulators of EC behaviours and angiogenic capacity. The following section examines how ECs perceive and transduce these mechanical signals.

### 3. Material mechanics and its effects on vascularization

#### 3.1 Stiffness

Matrix stiffness is a potent cue for EC behaviours and refers to a material's inherent resistance to deformation when subjected to an applied force. Stiffness is typically quantified by the Young's modulus ( $E$ ), or storage modulus ( $G'$ ), with the latter reflecting the elastic component of a viscoelastic material under oscillatory loading. In 2D systems, ECs on stiffer substrates generally form stable adhesions and generate stronger traction forces that facilitate cytoskeletal organization and capillary-like structures.<sup>78</sup> These mechanical cues are converted into intracellular signals through interconnected molecular mechanisms involving integrin clustering, cytoskeletal contractility, and transcriptional regulation as shown in Fig. 1. Specifically, stiff substrates enhance integrin-dependent activation of focal adhesion kinase (FAK) by promoting the engagement of matrix-binding integrins that recruit and activate FAK within focal adhesions, leading to its autophosphorylation and downstream signalling. Integrin-linked kinase (ILK) is a focal adhesion protein that transmits mechanical cues by interacting with integrins and linking them to Wnt/ $\beta$ -catenin and protein kinase B (Akt) signalling pathways. Altogether, integrin-FAK-ILK complexes are the major "load sensors" that convert matrix stiffness into biochemical signals for EC proliferation, migration, and survival.<sup>79,80</sup>

Matrix stiffness also increases EC contractility and stress fibre formation by elevating Ras homolog family member A (RhoA) GTPase activity and its effector Rho-associated kinase (ROCK).<sup>81,82</sup> The increased contractility, together with increased FAK phosphorylation, promotes nuclear translocation of Yes-associated protein (YAP) and transcriptional co-activator with PDZ-binding motif (TAZ) (YAP/TAZ), which drive the expression of genes that promote cell growth and angiogenesis (e.g., CYR61, CTGF, ANKRD1).<sup>83–86</sup> Elevated contractility also activates the myocardin-related transcription factor/serum response factor pathway (MRTF/SRF), which shifts ECs toward a more motile and invasive phenotype. Notably, in stiffened matrix, SRF activity has been shown to selectively regulate EC tip cell invasion.<sup>87,88</sup> *In vivo*, knockout of SRF inhibits tip-cell



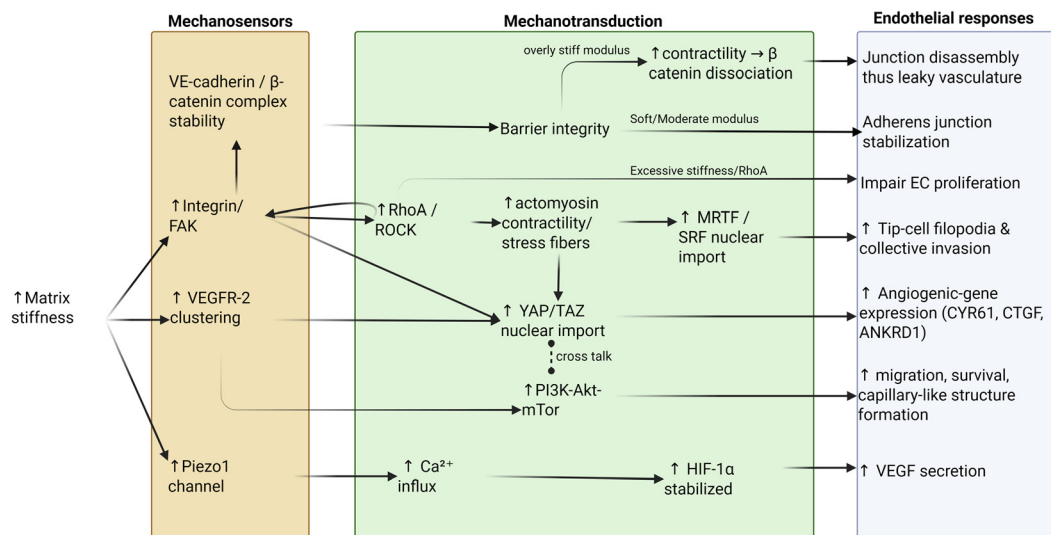


**Fig. 1** Mechanosensing pathways of endothelial cells (ECs) on 2D matrix. Increased matrix stiffness is sensed by ECs through integrin/FAK signalling, VEGFR2 organization, and the mechanosensitive channel Piezo. Integrin/FAK activation enhances RhoA/ROCK-dependent actomyosin contractility and stress-fibre formation, promoting nuclear translocation of YAP/TAZ and MRTF/SRF and coordinating pro-angiogenic transcriptional factors. Stiffness-associated signalling also engages PI3K-Akt-mTOR; context-dependent crosstalk between the YAP/TAZ and PI3K pathways supports migration, survival, and morphogenesis. Matrix stiffness modulates barrier integrity via VE-cadherin/ $\beta$ -catenin stability: soft-to-moderate stiffness favours adherens junction stabilization, whereas excessive stiffness elevates contractility, promotes junction disassembly, and increases vascular leakiness. Piezo1-mediated  $\text{Ca}^{2+}$  influx can stabilize HIF-1 $\alpha$  and stimulate the expression of pro-angiogenic factors (Fig. 1 drawn by the author).

filopodia formation and severely impairs sprouting angiogenesis.<sup>87,89</sup> Beyond integrin-based mechanosensing, Piezo1 is a mechanosensitive cation channel in ECs that opens in response to membrane tension, allowing  $\text{Ca}^{2+}$  influx and supporting endothelial migration and angiogenesis.<sup>90–93</sup> This influx has been shown to stabilize HIF-1 $\alpha$  and drive pro-angiogenic factors vascular endothelial growth factor (VEGF) and angiopoietin 2 (ANGPT2) expression in mice and lymphatic endothelial cells, as well as gastric cancer cells.<sup>94–97</sup> Conversely, while high stiffness promotes angiogenesis, excessive rigidity can impair vascular network formation through multiple mechanisms. Over-activation of RhoA has been shown to impair EC proliferation, migration and tube formation.<sup>82,98,99</sup> As stiffness-induced actomyosin contractility rises ( $E \geq 10$  kPa), the vascular endothelial cadherin (VE-cadherin)/ $\beta$ -catenin-based adherens junction becomes destabilized via FAK/Src-dependent phosphorylation, leading to junction disassembly, increased endothelial permeability, and impaired network formation.<sup>100,101</sup> Conversely, on softer matrices (2.5 kPa),<sup>100,101</sup> ECs maintain strong VE-cadherin/ $\beta$ -catenin junctions, which supports barrier function and morphogenesis. Chronic YAP activation can also contribute to negative outcomes, such as pathologic fibrosis in wound healing contexts.<sup>83</sup>

Beyond driving pro-angiogenic gene expression, matrix stiffness also primes endothelial cells to respond more effectively to soluble growth factors. VEGF-A binding to its receptors (VEGFR-1 and VEGFR-2) is a central step in angiogenesis. Crucially, matrix stiffness modulates this process by regulating VEGF-A secretion, VEGFR-2 receptor dynamics, and down-

stream signalling.<sup>102,103</sup> For example, ECs on  $E = 10$  kPa hydrogels display higher p-ERK1/2 levels and VEGFR-2 endocytosis than those on  $E = 1$  kPa gels.<sup>103</sup> Beyond these receptor dynamics, the availability of VEGF itself can act as a dominant regulator of endothelial morphogenesis. Specifically, in a thiol-modified HA gelatin hydrogel system spanning 10 to 650 Pa, high VEGF was required to initiate tube morphogenesis of endothelial progenitor cells. Under these conditions, tube morphogenesis increased as substrate stiffness decreased.<sup>104</sup> Importantly, this stiffness potentiation of VEGF signalling is most evident in nascent or sparse ECs, whereas strong adherens contacts override matrix cues.<sup>103</sup> Substrate stiffness and VEGFR-2 converge on the phosphoinositide 3-kinase (PI3K)-Akt-mechanistic target of rapamycin (mTOR) signalling pathway, promoting migration and capillary-like structure formation. Inhibiting mTOR reduces stiffness-driven signalling, reducing VEGF production and angiogenesis.<sup>102,105</sup>

Much of the mechanosensing framework has been established in 2D culture on planar substrates. However, translating these principles to 3D vascular models requires treating 'dimensionality' not as a single variable, but as a complex bundle of coupled microenvironmental differences. Because of this, cell-ECM mechanotransduction mechanisms in 3D often diverge from 2D observations.<sup>106,107</sup> Functional differences arise from distinct features of each context, including how adhesions and mechanical forces are spatially presented, how diffusible cues are regulated, and whether certain multicellular responses are even possible on planar substrates.<sup>106</sup> In 3D ECMs, mechanical confinement by the surrounding matrix restricts global changes in cell shape and volume, but cells can



still generate matrix stresses through protrusion extension, actomyosin-based contractility, and cell-volume regulation. Importantly, cell–matrix interactions become dynamic as the matrix is remodeled.<sup>107</sup> Furthermore, imaging and interpreting FA-based structures in 3D contexts is also more challenging because adhesions can be reduced in size or intensity and are harder to resolve in non-planar samples.<sup>106</sup> Specifically, 3D environments drive the formation of unique 3D-matrix adhesions that selectively rely on  $\alpha 5\beta 1$  and  $\alpha v\beta 3$  integrins and exhibit altered FAK phosphorylation compared to 2D focal adhesions. In this setting, stiffness must be interpreted alongside other matrix properties like viscoelasticity and degradability, and 3D mechanotransduction can proceed through both integrin-mediated pathways and mechanosensitive ion channels that respond to confinement.<sup>107</sup> For example, studies demonstrate that altering the stiffness of substrates like collagen-coated PAAm or 3D collagen gels simultaneously modifies architectural features such as porosity, anchoring distances, and binding-site density, which can independently alter focal adhesion formation and ERK/MAPK signalling.<sup>108,109</sup> The impact of this architecture is evident in heterogeneous 3D collagen, where local fibril bundling generates large adhesion-scale stiffness heterogeneity of up to 10 fold that directly modulates adhesion stabilization.<sup>110</sup> Unlike in 2D globular collagen, where myosin II inhibition with blebbistatin reduces  $\beta 1$  integrin activation and clustering, activated  $\beta 1$  integrins in native 3D fibrillar collagen remain clustered even under blebbistatin. This indicates that the fibrillar micro-architecture itself can physically sustain integrin organization even with reduced contractile input. ECs further illustrate how these dimensional factors gate complex mechanobiological outputs. Microvascular ECs cultured in 3D type I collagen lattices show increased MMP-2 activation and upregulate MT1-MMP compared to 2D monolayers. While broad-spectrum MMP inhibition produces no noticeable change in 2D monolayer morphology or behaviour, MT1-MMP-dependent proteolysis and its subsequent Cdc42 activation are strictly required for multicellular network establishment, endothelial lumen formation, and vascular guidance tunnel generation in 3D matrices.<sup>110–112</sup> Finally, transcriptomic comparisons demonstrate that VEGF induces a broader response in 3D spheroid sprouting than in 2D wound-healing and proliferation assays, with pronounced changes in cell–matrix interaction, glycolysis, and tip and stalk signatures uniquely evident in 3D.<sup>113</sup>

Within 3D matrices, EC migration occurs collectively with cells connected in clusters or chains as they form vessel-like structures. In soft matrix environments, the ECM more easily yields to cell-generated force, preventing the buildup of strong tension at integrin-based adhesion sites. Thus, integrin bonds follow a “catch-bond” mechanism where mechanical tension prolongs bond lifetimes. The relatively low stress on a soft substrate causes these bonds to remain transient and disassemble more readily, permitting cell rearrangement and aggregation;<sup>114</sup> conversely in stiff environments, cells remain anchored due to stronger focal adhesions. Furthermore, increasing matrix stiffness often envelops the cells in a denser

polymer network which resists remodelling, physically confining cells into rounded morphologies and inhibiting YAP nuclear translocation.<sup>115</sup> Similarly, studies which created dynamic stiffening gels showed a dissociation of  $\beta$ -catenin from VE-cadherin and destabilization of adherens junctions as stiffness increased, which is associated with altered vascular network morphology.<sup>116,117</sup> Conversely on softer gel, VE-cadherin and  $\beta$ -catenin remain more strongly co-localized at endothelial junctions. Comparatively, studies on 2D human umbilical vein endothelial cell (HUVEC) monolayers cultured on collagen-coated PA gels show that increasing the stiffness from 2.5 to 10 kPa promotes VE-cadherin phosphorylation, widens junctions, and reduces junctional  $\beta$ -catenin levels *via* FAK-dependent signalling that promotes Src recruitment to adherens junctions.<sup>100</sup> Consistent with this, inhibiting ROCK on stiff substrates rescues migration<sup>118</sup> indicating that reducing ROCK-driven actomyosin tension can partially override “stiff-substrate” behaviour. ECs also actively remodel their surroundings through protease-mediated ECM degradation. For example, ECs embedded in softer 3D matrices ( $E = 2$  kPa) have increased matrix metalloproteinase (MMP) secretion and activation, facilitating efficient ECM remodelling and promoting cell migration compared to those in stiffer matrices ( $E = 15$  kPa).<sup>119,120</sup> This MMP-driven remodelling in softer hydrogels supports the formation of prevascular EC networks and improved perfusion *in vivo*.<sup>120</sup> Finally, unlike in 2D culture, alterations in matrix stiffness in 3D are often accompanied by concurrent changes in other physical properties, including polymer density, porosity, and viscoelasticity, making it challenging to isolate the effects of stiffness alone. Altogether, these findings underscore that 3D hydrogel matrices are not simply thicker 2D substrates but present a fundamentally distinct mechanical and biochemical context that must be deliberately engineered to study and direct endothelial vascularization. Consistent with these context-dependent differences, in 2D environments, moderate matrix stiffness has been reported to promote integrin/FAK and YAP/TAZ pathways that stabilize adherens junctions and provide traction for migration, whereas pathological stiffening hyperactivates RhoA/ROCK and disrupts barrier integrity. Conversely, in 3D matrices, soft environments permit protease-driven matrix yielding for robust network assembly, while increased stiffness imposes steric confinement that restricts YAP translocation and inhibits capillary morphogenesis.

*In vivo* evidence suggests the existence of a mechanically optimal stiffness range for vascularization rather than a simple softer or stiffer relationship. For example, in one silk-fibroin scaffolds study, a compressive modulus of 5.7 kPa was associated with the greatest vascular ingrowth (around 70 vessels per  $\text{mm}^2$ ), whereas both lower (3 kPa) and higher (15.3 kPa) modulus scaffolds were less supportive.<sup>121</sup> In parallel, collagen cross-linking studies show that stiffening ECM can also shift vascular phenotype rather than simply increase vessel number, for example by increasing angiogenic branching while also destabilizing endothelial junctions and increasing permeability, consistent with the altered VE-cadherin/



$\beta$ -catenin organization mentioned above.<sup>78</sup> Furthermore, the mechanical properties of the infarct zone evolve rapidly from a soft provisional matrix to a stiff fibrotic scar over weeks. Therefore, a hydrogel optimized for a single stiffness value may be most permissive for vascularization only during a limited therapeutic window and could become progressively mismatched with the remodelling myocardium. This highlights the potential value of hydrogels with dynamically tunable stiffness that can change in concert with the healing infarct region.

### 3.2 Viscoelasticity, plasticity, and stress relaxation

Viscoelasticity is a key biophysical feature of native tissues. It describes the time-dependent mechanical behaviour of materials combining both elastic and viscous responses, enabling them to resist stress, deform over time, and recover upon stress removal. Key parameters include storage modulus ( $G'$ ), loss modulus ( $G''$ ), and the loss tangent ( $\tan \delta = G''/G'$ ) and stress relaxation time ( $\tau_{1/2}$ ), which quantifies how rapidly internal stress dissipates under constant strain. Native soft tissues have stress relaxation times ranging from tens to hundreds of seconds.<sup>122</sup>

With increasing recognition of viscoelasticity as a regulator of cell behaviour, recent advances have focused on designing viscoelastic hydrogels. Viscoelastic hydrogels can be synthesized by physical crosslinking (e.g. ionic, hydrogen-bond, hydrophobic, or host-guest interactions)<sup>123</sup> or dynamic crosslinking (e.g. Schiff bases, hydrazones, borate esters), as reviewed elsewhere.<sup>62,81,124</sup> Alternatively, interpenetrating networks combine a permanent covalent network for structural integrity with a dynamic (physical or covalent) dissipative network, achieving tissue-mimetic toughness for load-bearing applications.<sup>125–128</sup> These viscoelastic hydrogels can be engineered with a tunable  $\tau_{1/2}$ , the time to decay to 50% of the initial stress, to regulate vasculature formation. In general, intermediate/fast relaxation of the order of tens of seconds to minutes favors 3D vasculogenesis and angiogenic sprouting, and various notable experiments found that stress relaxation windows within hundreds of seconds promote angiogenesis.<sup>129–131</sup> For example, low stiffness elastin-like peptide (ELP) hydrogels with fast relaxing increased branch length by 33% and branch width by 57%, compared to slow-relaxing, same-stiffness analogues.<sup>130</sup>

These benefits are mainly correlated with heightened FAK activation *via* integrin  $\beta 1$  clustering and vinculin recruitment,<sup>131,132</sup> leading to myosin light chain phosphorylation (pMLC), its localization into the actin cytoskeleton, and subsequent actin contraction, protrusions, and filopodia formation.<sup>131,133</sup> FAK signalling activates multiple downstream pathways that collectively support angiogenesis. It increases both MRTF/SRF and YAP/TAZ to drive the transcription of cytoskeletal and adhesion genes and engages PI3K/Akt/mTOR signalling to further support YAP activity,<sup>134,135</sup> proliferation, and survival.<sup>136</sup> FAK signalling also upregulates MMP secretion (MT1-MMP, MMP9, and MMP1), promoting ECM degradation and remodelling, enabling sprouting, branching, and vascular

bed formation.<sup>81,89,131</sup> Mechanistically, endothelial tubulogenesis in 3D matrices is tightly coupled to matrix proteolytic permissiveness. MT1-MMP operates in concert with Rho GTPase signalling to support endothelial invasion, lumen formation and the generation of proteolytically carved “vascular guidance tunnel” spaces that enable subsequent remodelling.<sup>137</sup> Moreover, it has been shown that viscoelastic gels allow cells to migrate independently of MMP, where invadopodia exert protrusive and contractile forces to mechanically open channels, bypassing the need for ECM degradation.<sup>138</sup> This migration is  $\beta 1$  integrin-, Arp2/3-, and Rac1-dependent but does not require MMP activity. Conversely, when FAK signalling is inhibited, upregulation of MT1-MMP, MMP1, and MMP9 is reduced and downstream FAK/Src activation is limited, yielding rounded, non-migratory ECs with negligible sprouting.<sup>129</sup>

*In vivo*, the same fast-relaxing formulation doubled the microvessel density, confirming that hydrazone dynamics, rather than stiffness alone, drives endothelial morphogenesis.<sup>129</sup> Thus, tuning stress relaxation kinetics is important as intermediate relaxation supports angiogenesis, whereas overly fast or overly slow relaxation can destabilize cell-cell adhesion and impede functional vasculogenesis. Shayan *et al.* showed in a subcutaneous implantation model that fast-relaxing, low-stiffness hydrogels supported greater vascularization than their slow-relaxing counterparts, increasing the microvascular density from  $5.4 \pm 0.1$  to  $9.3 \pm 2.0$  vessels per  $\text{mm}^2$ .<sup>129</sup> Similarly, in a rat MI model, Sun *et al.* found that a dynamic viscoelastic hydrogel increased arteriole density in the infarct zone, indicating that viscoelasticity also affects post-MI vascular maturation toward smooth muscle-associated arteriole-like vessels rather than simply an increase in capillary number.<sup>139</sup> Despite these encouraging findings, the native myocardium has a fibrillar structure and exhibits anisotropic stress relaxation that the current isotropic hydrogel systems do not fully capture. Furthermore, stress relaxation profiles optimized under *in vitro* conditions may behave differently under the cyclic mechanical loading of the beating heart, where dynamic compression and shear act continuously on implanted materials.

In addition, many hydrogels also exhibit mechanical plasticity, which is a permanent residual deformation after cyclic mechanical loading/unloading arising from bond rupture/reformation or network rearrangement. Plasticity arises when networks contain bonds or topologies that can yield and reform (e.g., host-guest supramolecular bonds interpenetrated with a covalent network, or dynamic covalent chemistries such as imines/hydrazones in interpenetrating networks), and is typically determined by the non-recoverable deformation in creep-recovery tests and quantified by (permanent strain/maximum strain  $\times 100\%$ ).<sup>131</sup> Matrix plasticity has a biphasic effect on angiogenic and vasculogenic activities of ECs. In hydrogels engineered to span low (10% plasticity), medium (25% plasticity), and high-plasticity (50% plasticity) with a similar  $G'$ , medium plasticity maximized EC invasion distance, branching, and lumenization. In highly plastic matrices, large



irreversible deformations and network collapse are accompanied by elevated EC contractility and reduced vascular stability.<sup>132</sup> This is due to matrices that are easily permanently deformed, dissipating traction forces too quickly, which compromises vascular structures leading to premature gel collapse, EC hypercontractility, and fragmented, non-perfusible networks. Mechanistically, this phenotype is associated with excessive integrin-FAK signalling, heightened phosphorylated myosin light chain activity (pMLC), and junctional breakdown *via* VE-cadherin loss and  $\beta$ -catenin displacement. Conversely, low-plasticity matrices inhibit angiogenesis, which is associated with their resistance opposing cell-driven matrix deformation. As a result, integrins cluster poorly and FAK/Src activation is limited, yielding rounded, non-migratory ECs with negligible sprouting.<sup>131,132</sup>

Altogether, these findings suggest that endothelial responses to viscoelastic hydrogels depend on balancing stress relaxation with sufficient matrix stability. Within this framework, appropriately fast or intermediate relaxing matrices promote  $\beta$ 1-integrin clustering and FAK/pMLC signalling, supporting protrusion formation and MT1-MMP-linked remodelling or invadopodia-mediated channel opening that increases branching and network formation. At the extremes, slow/non-relaxing gels limit integrin clustering and sprouting, while highly plastic matrices dissipate traction too quickly, driving hypercontractility, junctional breakdown, and premature network collapse.

### 3.3 Matrix degradability and porosity

Matrix degradability is a vital determinant of EC morphogenesis. During angiogenesis in native tissue, endothelial tip cells secrete proteases to digest the basement membrane and interstitial matrix, clearing a path for sprouts. If the matrix is non-degradable, ECs often cannot progress to form tubules or networks.<sup>119,140</sup> To facilitate sprouting angiogenesis, enzyme-cleavable crosslinks or labile bonds can be introduced. Beamish *et al.* directly compared hydrogels with different degradability using a PEG gel containing an MMP-cleavable peptide (VPMS) or a plasmin-cleavable peptide (YKNR). MMP-degradable hydrogels supported robust capillary network formation across a range of crosslink densities. In contrast, plasmin-sensitive (but MMP-inert) YKNR gels permitted sparse and primitive capillary structures only at the lowest storage modulus (27 mg mL<sup>-1</sup> YKNR,  $G' = 40\text{--}60$  Pa), where total vessel length remained significantly lower than in the density-matched MMP-cleavable matrix. At higher polymer concentrations (32–40 mg mL<sup>-1</sup>) and in inert gels no capillary morphogenesis was observed (Fig. 2A).<sup>140</sup> Furthermore, protease requirements depend on the ECM context such as appropriate peptide sequences that are specifically susceptible to degradation. For example, the peptide sequence VPMSMRGG demonstrates susceptibility to degradation by MMP-1, leading to faster ECM remodelling compared to other sequences.<sup>141,142</sup> Conversely, using a less suitable or MMP-inert peptide sequence significantly impedes the degradation process, hindering EC migration, remodelling capacity, and capillary mor-

phogenesis.<sup>140</sup> Conversely, if a matrix is excessively soft and degrades too rapidly, loss of mechanical integrity may compromise the stability of the initially formed vascular networks and promote their regression.<sup>143</sup> Therefore, tailored peptide crosslinks matching the enzymatic degradation profiles of EC-secreted proteases are vital for effective, targeted, and organized capillary morphogenesis in 3D hydrogels.

In addition to matrix degradation, matrix porosity, including the size and connectivity of pores in both engineered and native matrices, critically dictates how ECs sense and navigate through the matrix. In conventional cell-laden hydrogels, the mesh pore size is in the order of nanometres, far smaller than a cell, and thus ECs must rely on proteolytic remodelling, matrix plasticity or viscoelastic yielding to create paths for sprouting by mechanical deformation.<sup>138,147</sup> In contrast, hydrogels engineered with an initial microporosity of tens to hundreds of  $\mu\text{m}$  permit more immediate cell invasion. Many have reported that ECs and supportive cells can migrate in a protease-independent manner when the pore sizes approximate the cell diameter.<sup>138,148,149</sup> Chiu *et al.* observed that in PEG hydrogels with 25–50  $\mu\text{m}$  pores, endothelial invasion was mostly confined to the outer surface; by increasing the pore size to 50–150  $\mu\text{m}$ , robust vascular ingrowth occurred throughout the scaffold (Fig. 2C).<sup>145</sup> Similarly, CD31 immunofluorescence of HUVECs on  $\beta$ -TCP scaffolds with 100, 120, or 150  $\mu\text{m}$  interconnections at 7 and 14 days showed increased CD31 over time, with multicellular networks evident by day 14 in the 150  $\mu\text{m}$  group, whereas network structures were less apparent in the 100–120  $\mu\text{m}$  groups.<sup>144</sup>

Porosity within hydrogels can be engineered through several fabrication techniques, including variations in polymer concentration, crosslink density, sacrificial templating, and cryogelation methods. However, adjusting the porosity often has a significant impact on the material's mechanical properties; for example increased polymer content or crosslinking typically reduces pore size, diffusivity, porosity and viscoelasticity while enhancing stiffness (Fig. 2E).<sup>146,150</sup> Alternatively, sacrificial templates or porogens, such as salt crystals, degradable microspheres or microparticles are incorporated during hydrogel synthesis and later removed *via* leaching or enzymatic degradation to create predefined, interconnected macroporous structures. However, this approach can modestly reduce the bulk stiffness depending on pore size and volume fraction. For example, using gelatin microspheres of  $248 \pm 44$   $\mu\text{m}$  from heparin-hyaluronic acid (HepHA) gels yielded macroporous scaffolds, which significantly increased HUVEC migration and produced the most pronounced vascularization *in vitro* and *in vivo*. However, the compressive modulus decreased modestly.<sup>151</sup> The mechanical deficit can be compensated by dispersing stiff nanofillers, such as graphene oxide/LAPONITE®,<sup>152</sup> or by integrating fibrous reinforcement 3D-printed microfibrils or electrospun yarns. For example, embedding melt-electrospun polycaprolactone (PCL) microfibrils (93–98% porosity) into hydrogels increased the compressive stiffness 54-fold while maintaining pore interconnectivity for cell migration.<sup>153</sup> Similarly, poly(L-lactic acid) (PLLA) yarn-reinforced gelatin



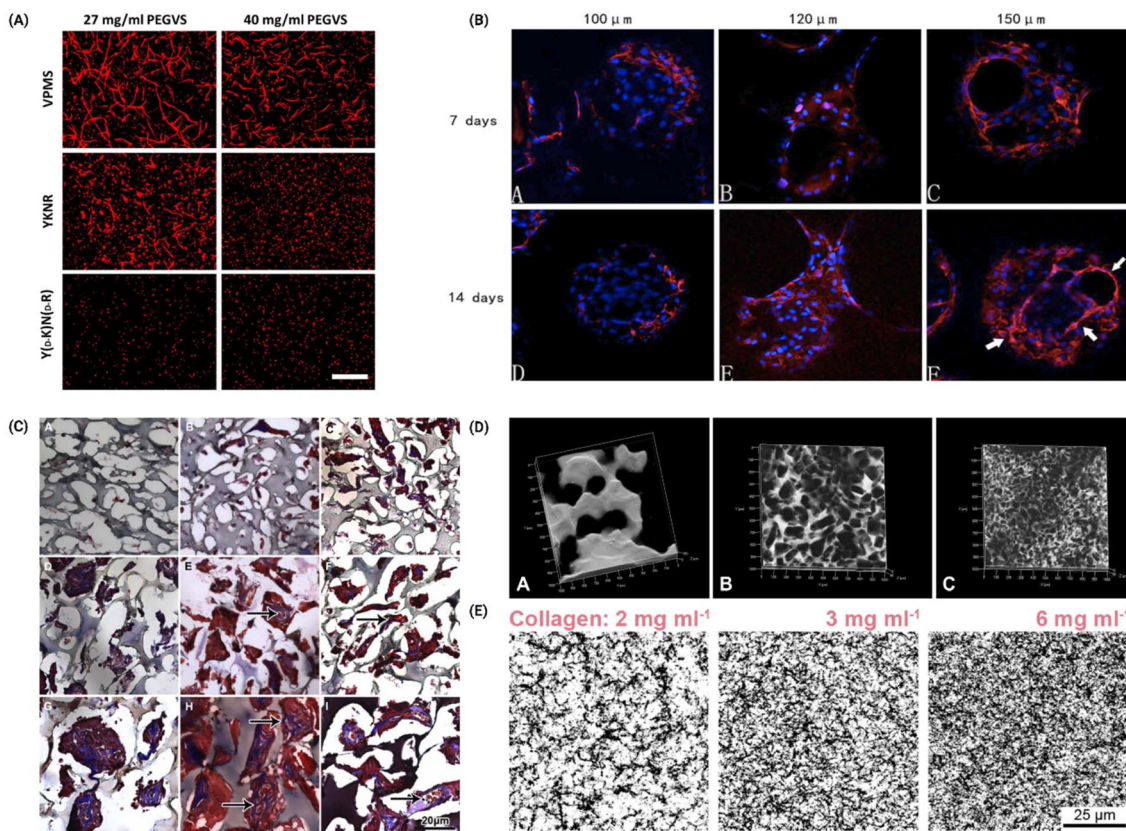


**Fig. 2** Architectural control of endothelial activation and vascularization *via* scaffold porosity and degradability. (A) Endothelial-fibroblast co-cultures in PEG-VS hydrogels with MMP-sensitive (VPMS), plasmin-sensitive (YKNR), or non-degradable ( $Y_D$ ,  $KN_D$ ,  $R$ ) crosslinks at 27 or 40 mg mL<sup>-1</sup>. UEA-lectin staining (red) shows capillary networks. Adapted from ref. 140 with permission from Wiley Periodicals, Inc, copyright 2019. (B) PECAM-1 (CD31) immunofluorescence of HUVECs on beta-tricalcium phosphate ( $\beta$ -TCP) scaffolds with 100, 120, or 150  $\mu$ m interconnections at 7 and 14 days. Cell-cell CD31 increases over time and is most robust on 150  $\mu$ m scaffolds, where multicellular networks appear by day 14, marked by arrows. Adapted from ref. 144 (Copyright 2025, Xiao *et al.*) and is open access. (C) Masson's trichrome staining of porous gels 1 (A, D and G), 2 (B, E and H), and 3 (C, F and I) weeks post-implantation. Panels show pore ranges 25–50  $\mu$ m (A–C), 50–100  $\mu$ m (D–F), and 100–150  $\mu$ m (G–I). Vascularized (arrow) collagen (blue) is evident in medium (D–F) and large (G–I) pores at all time points. (D) Confocal volume renderings of PEG hydrogels with salt-templated pores (A: 100–150; B: 50–100; C: 15–50  $\mu$ m). Pores (FITC-protein-filled) shown black after inversion; hydrogel matrix white. (C) and (D) Adapted from ref. 145 with permission from Elsevier, copyright 2011. (E) Collagen pore sizes are changed due to a change in matrix density. Adapted from ref. 146 with permission from Elsevier, copyright 2011.

hydrogels exhibited 10-fold higher tensile strength and enhanced fibroblast adhesion despite reduced pore size.<sup>154</sup> Another method of creating porous materials is cryogelation, which utilizes ice crystal formation to template interconnected macropores of typically 50–200  $\mu$ m. This process often preserves mechanical stability by forming crosslinked polymer walls around ice porogens, minimizing compressive modulus loss.<sup>155</sup> In Dong *et al.*'s design, gelatin methacryloyl (GelMA)/poly(ethylene glycol) diacrylate (PEGDA) cryogels on sulfonated LCFRPEEK implants achieved 96  $\mu$ m pores, which approximately doubled HUVEC infiltration compared with the non-porous control and increased angiogenesis.<sup>156</sup> However, due to the random nature of freezing, the pore size was heterogeneous ( $\pm 28.98$   $\mu$ m standard deviation). Moreover, while stiffness integrity remained constant, drying methods often compromise mechanical resilience, leading to brittleness, pore collapse, or poor elasticity, which limits functional deployment in dynamic tissues such as the heart.<sup>157,158</sup> These structural

limitations are repaired by incorporating an elastomeric PEG-PCL backbone, yielding salt-leached scaffolds with recoverable elasticity and handling strength.<sup>159</sup>

In summary, matrices engineered with MMP-cleavable crosslinks or initial macroporosity support protease-dependent and contact-driven migration pathways, enabling tip cells to overcome steric barriers for infiltration and capillary morphogenesis. Conversely, non-degradable or nanoporous environments can impose severe steric hindrance, limiting invasion to the matrix surface and markedly restricting multicellular network assembly. However, in the *in vivo* setting, degradation rates optimized *in vitro* may not directly translate, as the inflammatory environment, macrophage-mediated degradation, and MMP activity differ substantially from controlled culture conditions. Matching degradation kinetics to the pace of vascular ingrowth and tissue remodelling in the infarcted myocardium, which itself evolves over weeks, therefore remains an important design consideration.



### 3.4 Anisotropy

The native myocardium exhibits intrinsic anisotropy defined by the alignment of cardiomyocytes and ECM, resulting in direction-dependent mechanical properties.<sup>160</sup> The longitudinal-to-transverse stiffness ( $E_{\text{longitudinal}}/E_{\text{transverse}}$ ) typically ranges from 2 to 3, and fibre orientation angles vary across the ventricular wall to optimize the electromechanical coupling.<sup>161</sup> After MI, the natural anisotropic fibre alignment of heart tissue is disrupted. This leads to mechanical stiffening, impaired contraction, and disorganized electrical propagation, contributing to conduction abnormalities and heart failure.<sup>162</sup> These changes may also reduce nascent capillaries of the aligned guidance cues that normally orient endothelial sprouting parallel to muscle fibres, thereby slowing reparative angiogenesis.

Engineered anisotropy in biomaterials has been shown to recreate aspects of these directional cues and support vascular organization. On 2D substrates, ridge/groove patterns can direct EC migration and the orientation of new vessels by contact guidance.<sup>163</sup> Suarez *et al.* showed that the ridge/groove size of a substrate dramatically affects network formation.<sup>164</sup> On nanopatterns, ECs were able to connect and form capillary-like networks, albeit initially unstable, whereas on micropatterned grooves (1.5–9.9  $\mu\text{m}$  scale), ECs tended to align along the patterns but failed to interconnect into networks.<sup>164</sup> In 3D environments, topographical cues arise from the matrix microstructure. Native collagen and fibrin hydrogels provide contact guidance for EC sprouting through their fibrous mesh, where aligned fibre matrices lead to anisotropic, parallel capillary orientation while isotropic fibre networks yield randomly interconnected capillary meshes.<sup>165,166</sup> To mimic native fibrous ECM, electrospun nanofibres have been embedded within hydrogels.<sup>167</sup> The presence of these embedded fibres provided a 3D topographic framework that guided cell organization and modulated the mechanical properties, for example by increasing tensile strength along the fibre direction. The aligned nanofibres orient the cells and create provisional guidance channels for new vessels, while the surrounding hydrogel supported cell infiltration. Beyond fibre organization, pre-formed microchannels within a hydrogel serve as templates that ECs can quickly line and turn into perfusable vessels.

At the molecular level, aligned collagen or nanofibrillar scaffolds organise paxillin into elongated focal adhesions,<sup>168</sup> engaging FAK mechanosignalling and activating downstream PI3K/Akt and the RhoA/ROCK-myosin-II pathways. These cascades reinforce actin stress-fibres and directional traction. Pharmacological blockade of FAK (FI-14), ROCK (Y-27632) or myosin-II (blebbistatin) attenuates these effects, suggesting a mechanotransductive contribution to endothelial responses to anisotropic collagen.<sup>169,170</sup> Contact guidance is the macroscopic outcome of this signalling where in nanofibrillar collagen (cell alignment = 0.6) EC protrusions migrate 4.3-fold faster along the fibre axis than perpendicular to it.<sup>169</sup> Mechanistically, this process has been proposed to rely on integrin-generated tension that propagates to adherens junc-

tions, where  $\beta$ 1-integrin-dependent actomyosin contractility stabilises VE-cadherin- $\beta$ -catenin complexes and supports sprout extension.<sup>171</sup>

Multiple fabrication strategies enable precise control over material anisotropy, including electrospinning, photolithography, bio-templating, and microfluidic flow-induced alignment. For example, electrospinning using a “ridge-valley” spring collector produced poly(D,L-lactic acid) (PDLLA)/PCL/gelatin fibrous scaffolds with longitudinal-to-transverse modulus ratio up to 3. On these scaffolds, VEGF, VE-cadherin and eNOS were upregulated, resulting in increased EC proliferation compared with random-fibre mats.<sup>172</sup> Similarly, field-induced alignment can be used to orient charged or magnetic fillers before gelation. For example, a silk-chitosan pre-gel with polarized fibres prepared by alternating current electric fields-induced fibre alignment and anisotropic conductive hydrogels using magnetically aligned  $\text{Fe}_3\text{O}_4$  nanoparticles embedded in GelMA both improved cellular alignment and supported vascularization.<sup>173,174</sup> Microfluidic shear printing has emerged as a direct way to impose fibre alignment. Extruding a poly(3-hydroxybutyrate-4-hydroxybutyrate)/PCL bio-ink through a microfluidic print-head yielded strictly parallel filaments that improved HUVEC metabolic activity and enhanced *in vivo* angiogenesis.<sup>175</sup>

Bio-templating exploits native tissues that already possess anisotropic micro-architecture with direction-dependent stiffness that better matches the beating myocardium. For example, Song *et al.* processed fish swim bladder collagen into an anisotropic hydrogel patch with tunable directional stiffness (*e.g.*,  $E = 212$  kPa parallel *vs.*  $E = 51$  kPa perpendicular to fibres) and strong resilience under cyclic tensile loading.<sup>176</sup> Similarly, Liang *et al.* leveraged aligned plant cellulose to create an anisotropic electroactive hydrogel that served as an epicardial patch for cardiac repair.<sup>177</sup> Both methods significantly improved cardiomyocyte alignment, survival, angiogenesis, electrical integration, and functional recovery in MI models by recreating microstructurally anisotropic mechanical-electrical microenvironment that closely matches native myocardium. Altogether, these findings demonstrate that bio-templated anisotropic matrices can promote vascularization and cardiac repair; however, their specific effects on capillary morphogenesis *in vivo* remain largely untested.

In summary, aligned topography provides contact guidance by organizing elongated focal adhesions and engaging FAK-PI3K/Akt and actomyosin tension, which can accelerate directional migration and promotes parallelized vessel architectures. In isotropic matrices, symmetric adhesion and force distribution more often yield randomly oriented, highly interconnected meshes with reduced higher order organization.

## 4. Hydrogel matrix materials

Hydrogels provide mechanically tunable, biomimetic scaffolds that both model and promote post-MI neovascularization. By tailoring stiffness, viscoelastic stress-relaxation, and per-



meability, injectable gels can match the mechanics of native myocardium and have been shown to accelerate arteriogenesis in large-animal MI models.<sup>178–180</sup> Cell-laden hydrogels, or matrices infused with endothelial-cell extracellular vesicles, form living constructs that anastomose with host vasculature and mature into perfused microvessels. Crucially, the base polymer's mechanics, degradability and ligand density gate EC adhesion, migration and lumen formation, making the material choice as important as the bioactive cargo delivered. Beyond injectable therapies, hydrogels also enable *in vitro* models that recapitulate vessel-wall architecture, impose physiological shear, enable barrier-integrity and thrombosis assays, and support disease-specific or high-throughput drug screens.

#### 4.1 Natural ECM-derived hydrogels

**4.1.1 Collagen gels.** As the primary protein of cardiac ECM, collagen I is widely used to create hydrogels that mimic the myocardial matrix by providing cell-adhesive ligands and an architecturally fibrous scaffold.<sup>181–184</sup> ECs primarily interact with collagen I through the integrin receptor  $\alpha 2\beta 1$ ,<sup>185–187</sup> which plays an important role in mediating adhesion, migration, and angiogenesis within collagen-rich environments. Moreover, its inherent biodegradability due to its susceptibility to MMP-mediated breakdown allows for embedded endothelial cells to degrade collagen and carve out lumen space for vascular network formation.<sup>182,188</sup> Collagen I is typically isolated from rat tail or bovine skin as acid-soluble monomers, neutralized, and allowed to self-assemble into fibrils at 37 °C. Typical formulations for cardiac models use collagen concentrations of 1–3 mg mL<sup>-1</sup> (0.1–0.3% w/v). Although pure collagen I gels represent the fibrous environment of the heart, their storage modulus is in the order of 10–100 Pa ( $G'$ ), which is softer than healthy native heart ECM, and certainly much softer than fibrotic post-MI ECM. Thus, to stiffen collagen gels, they are often crosslinked chemically using glutaraldehyde,<sup>189,190</sup> genipin<sup>191–193</sup> or transglutaminase.<sup>194,195</sup>

Dynamically stiffening collagen hydrogels has been used to simulate age-related or post-infarct scar environments to study how ECs behave in an increasingly fibrotic stiffer environment.<sup>101</sup> This has been achieved by various methods such as photocrosslinking of collagen I/methacrylated HA gels with a ruthenium photoinitiator<sup>101</sup> ( $E = 100$  Pa to 180–240 Pa) or interpenetrating collagen–norbornene–HA networks whose stiffness is increased by introducing an additional peptide cross-linker under UV light.<sup>196</sup> Across these systems a trend emerges where a soft starting modulus ( $E = 0.1$ –3 kPa) increases sprouting, a moderate rise into the low-kPa range consolidates lumens and tightens VE-cadherin junctions but overshooting that window triggers contractility-mediated regression and VE-cadherin junction disruption due to the combination of low porosity and high stiffness ( $E = 14$ –32 kPa). In addition, collagen gels can also be combined with cardiac cells to model *in vitro* infarcts, enabling the observation of revascularization as fibroblasts deposit additional collagen and increase stiffness. For example, Sakaguchi *et al.* created triple-layer neonatal rat cardiac-cell sheets of cardiomyocytes,

ECs, and resident fibroblasts perfused on a collagen-I gel pre-cast with channels.<sup>197</sup> Within five days ECs sprouted into the gel, anastomosed with the channels and produced a perfusable microvascular tree.

**4.1.2 Fibrin hydrogels.** Fibrin is a natural provisional matrix formed during blood clotting and wound healing, making fibrin hydrogels highly relevant for vascularization models.<sup>198,199</sup> In cardiac tissue engineering, typical fibrin gels are made by mixing fibrinogen solutions with thrombin at the point of use; this yields a fibrous network that inherently supports angiogenesis as endothelial cells readily invade fibrin clots.<sup>200,201</sup> Furthermore, fibrin contains binding sites for growth factors like VEGF and basic FGF to promote angiogenesis.<sup>202–204</sup> This results in faster and more robust capillary formation. A study showed that when human ECs and mesenchymal cells were co-cultured, fibrin gels supported extensive, well-connected capillary networks within 7–10 days whereas collagen gels yielded only sparse tubes.<sup>205</sup>

However, fibrin gels are relatively weak due to being prone to degradation by plasmin, and they often represent the early wound matrix rather than a mature scar.<sup>206,207</sup> To address this, fibrin can be chemically modified to enhance its mechanics and stability. For example, covalently bonding PEG to fibrinogen increased the stability of fibrin gel, promoted the sustained release of encapsulated VEGF, and enhanced infarct neovascularization and tissue preservation in a rodent MI model.<sup>199</sup> Another approach is ECM–fibrin hybrid hydrogels. Williams *et al.* created scaffolds composed of decellularized cardiac ECM from adult rat hearts mixed into a fibrin gel and crosslinked with transglutaminase. In their formulation, the base fibrin gel (3 mg mL<sup>-1</sup> fibrinogen) had a Young's modulus of 2–3 kPa, but by adding a transglutaminase crosslinker at 12  $\mu$ g mL<sup>-1</sup> or 120  $\mu$ g mL<sup>-1</sup>, they were able to increase the gel stiffness to 14 kPa and 32 kPa, respectively, spanning the stiffness range of neonatal and adult myocardium.<sup>208</sup>

**4.1.3 Hyaluronic acid hydrogels.** HA is a naturally occurring GAG that is abundant in embryonic hearts and in healing infarcts.<sup>209</sup> It is highly tunable and have been widely explored to model vascularization, often in combination with other polymers.<sup>185,210,211</sup> A unique feature of HA is its interaction with cell surface receptors through CD44 and receptor for hyaluronic acid-mediated motility (RHAMM) and its molecular weight-dependent effects: high-molecular-weight HA is anti-angiogenic and anti-inflammatory, whereas low-molecular-weight HA fragments can stimulate angiogenesis by activating inflammatory cells.<sup>212–214</sup> This was demonstrated in a rat MI model, where HA oligosaccharide treatment polarized macrophages toward a reparative phenotype, leading to significantly enhanced neovascularization and improved cardiac function.<sup>215</sup>

HA hydrogels are particularly attractive for infarct injections because HA is biocompatible and chemically defined. HA gels can be engineered to be biodegradable by hyaluronidase or hydrolysis over weeks to months.<sup>216,217</sup> For example, Hanjaya-Putra *et al.* engineered an HA hydrogel with MMP-degradable crosslinks, demonstrating that spatially patterned MMP-sensi-



tive regions could direct where vessels form and how they branch.<sup>7</sup> Similarly, Li *et al.* developed an injectable methacrylated HA hydrogel crosslinked with MMP-2-sensitive peptides and incorporated Arg-Gly-Asp (RGD) peptides, achieving tunable stiffness ( $G' = 1\text{--}5$  kPa).<sup>218</sup>

The stiffness of HA-based hydrogels can be tuned by adjusting polymer concentration and crosslinking density. For example, photocrosslinked HA hydrogels formed from 5% (w/v) methacrylated hyaluronic acid (MeHA) with 15 min UV exposure have been used to yield gels with Young's modulus = 50 kPa, while reducing the HA macromer concentration to 1% or shortening the UV exposure to 5 min produces much softer matrices with moduli = 3–4 kPa, as demonstrated.<sup>219</sup> However, HA lacks intrinsic cell-adhesive domains and therefore requires incorporating collagen or adhesion peptides to improve cell attachment. Common bioactive ligands incorporated into HA hydrogels for EC attachment include integrin-binding sequences like Tyr-Ile-Gly-Ser-Arg (YIGSR),<sup>220</sup> RGD,<sup>218</sup> Gly-Phe-Hyp-Gly-Glu-Arg (GFOGER),<sup>221,222</sup> and heparin binding peptides (HBP),<sup>223,224</sup> as well as adding collagen.<sup>225–227</sup>

**4.1.4 Alginate hydrogels.** Alginate is a polysaccharide from algae composed of mannuronic and guluronic acid units that forms ionic hydrogels in the presence of divalent cations, such as  $\text{Ca}^{2+}$ .<sup>228–231</sup> Similar to HA, alginate lacks intrinsic cell-adhesive motifs; thus, angiogenesis-competent constructs often use co-cultures, ECM additives, or peptide grafting (*e.g.*, RGD) to support endothelial morphogenesis. For example, it has been shown that in a chronic MI model, RGD-modified alginate injected into the infarct significantly improved capillary density and left ventricular function relative to unmodified alginate and saline control respectively.<sup>232</sup>

The stiffness and viscoelasticity<sup>233</sup> of alginate gels can be tuned by varying the molecular weight or guluronic acid content of the polymer and by adjusting the concentration of crosslinking ions.<sup>233–235</sup> Higher guluronic content and more  $\text{Ca}^{2+}$  typically produce a stiffer, slower-degrading gel. The degradation and mechanical strength of alginate gels can also be modulated by mixing alginate with chitosan.<sup>236</sup> Injection of alginate hydrogels into the infarcted heart has shown success in preclinical studies. In an infarct injection context, typically a 1–2% (w/v) sodium alginate solution is prepared and mixed with calcium salts upon injection, causing *in situ* gelation within the heart muscle.<sup>237</sup> This strategy thickens the infarct wall, and preserves the ventricular dimensions and fractional shortening, and RGD grafting onto the alginate further boosts arteriolar density in the scar.<sup>238</sup>

**4.1.5 Decellularized myocardial matrix (dECM) hydrogels.** A major advance in myocardial ECM biomaterials has been the development of hydrogels derived from animal heart tissue. In a landmark study, Singelyn *et al.* showed that an injectable porcine decellularized myocardial matrix could self-assemble into a nanofibrous hydrogel *in vivo* and recruit endogenous cells.<sup>239</sup> Composition analyses show that these dECM hydrogels retain a multitude of cardiac ECM constituents of primarily collagen I and III, but also collagen IV, laminin, fibronectin, elastin, and glycosaminoglycans similar to native tissue.<sup>240–242</sup>

Moreover, since dECM inherently contains angiogenic factors,<sup>243</sup> dECM hydrogels act as reservoirs for matrix-bound growth factors such as VEGF and bFGF which can be released during scaffold degradation or remodelling, thereby providing additional pro-angiogenic signals to invading cells.<sup>244,245</sup> In preclinical models using dECM, ECs and smooth muscle cells migrated into the matrix, significantly increasing arteriole density within the infarct zone after injection,<sup>246,247</sup> demonstrating the pro-vasculogenic potential of dECM hydrogels in an MI model.

The stiffness of dECM hydrogels is typically low, with a storage modulus in the hundreds of Pascals, but they can be concentrated to alter the mechanics. For example, increasing the ECM concentration from 10 mg mL<sup>-1</sup> to 60 mg mL<sup>-1</sup> increases the gel stiffness from 84 Pa to 771 Pa.<sup>248</sup> Alternatively, stiffness can be increased by chemical crosslinking. For example, adding glutaraldehyde at 0.05–0.1% to the myocardial matrix raises the storage modulus by roughly an order of magnitude.<sup>249,250</sup> Overall, the dECM hydrogel can serve as a bioscaffold that integrates with host tissue by filling the wound and providing structural support to the ventricle, encouraging the ingrowth of blood vessels and cardiac cells. In both small- and large-animal models, injected myocardial matrix has been shown to increase vessel density and improve left ventricular function,<sup>248</sup> potentially due to retained ECM proteins (*e.g.*, collagens and proteoglycans) and matrix-bound signalling cues.

## 4.2 Synthetic hydrogels

PEG is a widely used synthetic polymer for cardiac scaffolds due to its biocompatibility and tuneable chemistry. In the unmodified state, PEG gels lack biological signals, allowing researchers to add biochemical functionalities and precisely tune the mechanical properties without other confounding cues.<sup>251</sup> PEG and multi-arm PEGs are typically chemically functionalized with diacrylate,<sup>252,253</sup> thiol, maleimide, vinyl-sulfone, and norbornene,<sup>254–256</sup> and crosslinked through photocrosslinking or click chemistry. By adjusting the concentration of PEG and the degree of crosslinking, one can create hydrogels ranging from very soft ( $E' < 1$  kPa) to quite stiff ( $E' > 50$  kPa), covering the spectrum from healthy myocardium to fibrotic scar in terms of stiffness. For example, Günay *et al.* photochemically tuned an anthracene-functionalised PEG hydrogel from  $E' = 10$  kPa to  $E' = 50$  kPa to model the stiffness of healthy myocardium and fibrotic scar by irradiating it with 365 nm light.<sup>257</sup> Crosslink density controlled by light exposure in photopolymerized PEG or by the ratio of reactive PEG end groups seems to be another critical parameter requiring precise tuning.<sup>253</sup> Higher crosslink density will result in higher stiffness and lower swelling which helps maintain structural integrity and mechanical strength. However, it can also restrict nutrient and waste transport.<sup>253,258</sup> Conversely, if the crosslink density is too low, the gel may swell excessively, potentially compromising its mechanical properties. For cardiac and vascularization studies, PEG hydrogels are often functionalized with cell-adhesive peptides (like RGD) or combined with ECM



**Table 2** Comparison of common hydrogel matrices for post-MI vascularization and cardiac repair

Hydrogel platform	Baseline stiffness range and ease of modification	Common tuning mechanisms	Adhesion & bioactivity	Suitability for MI application (pros & cons)
Collagen	$G'$ ~10–100 Pa; moderately tunable <sup>266</sup>	Concentration; fibrillogenesis conditions (pH/temperature/ionic strength); chemical crosslinkers (e.g., EDC/NHS, genipin) <sup>267</sup>	$\alpha 2\beta 1$ adhesion, MMP-degradable, unmodified supports EC migration/angiogenesis <sup>185–187</sup>	Pros: highly biomimetic, inherent bioactivity. Cons: poor mechanical strength, difficult to tune, potential immunogenicity.
Fibrin	~0.1–5 kPa ( $G'$ at 1–10 mg mL <sup>-1</sup> fibrinogen). Tunable but low upper modulus <sup>268</sup>	Fibrinogen & thrombin concentrations; pH/ionic strength; FXIIIa crosslinking; blends (e.g., fibrin–collagen). <sup>268</sup>	Pro-angiogenic, wound-like matrix, binds growth factors. Fast degradation without stabilization <sup>202–204</sup>	Pros: potentially pro-angiogenic, mimics wound healing. Cons: mechanically weak, degrades too rapidly for sustained support.
HA	No gel without crosslinking, highly tunable of Pa to 100+ kPa range <sup>269</sup>	Methacrylation + photopolymerization; thiol–norbornene click (NorHA, photo- or Michael-type); guest–host; enzymatic (HRP/H <sub>2</sub> O <sub>2</sub> ). <sup>269,270</sup>	High molecular weight HA anti-inflammatory, low weight stimulates angiogenesis with added adhesion cues <sup>212–214</sup>	Pros: highly tunable, can match myocardial stiffness, potential for shear-thinning. Cons: requires modification for adhesion (RGD) and crosslinking.
Alginate	1 kPa → >100+ kPa depending on G content & Ca <sup>2+</sup> /Ba <sup>2+</sup> <sup>235</sup>	Ionic crosslinking with divalent cations (Ca <sup>2+</sup> /Ba <sup>2+</sup> ); adjust M/G ratio & polymer % post covalent/ photocrosslink <sup>232</sup>	Cell-inert, requires added adhesion peptides or matrix proteins, with adhesion it supports vessel growth <sup>232</sup>	Pros: inexpensive, simple ionic gelation. Cons: bio-inert, brittle, unstable crosslinks <i>in vivo</i> .
dECM	Soft gel of <0.5 kPa depending on content, difficult to tune <sup>271</sup>	Protein concentration; blending (e.g., with collagen/gelMA)	Native-like heart matrix, releases pro-angiogenic cues as it degrades, recruits vessels, increases arterioles <sup>240–242</sup>	Pros: unmatched biomimicry and bioactivity. Cons: mechanically very weak, batch variability, potential immunogenicity.
PEG	No gel without crosslinking; highly tunable across a range from Pa to >100 kPa (ref. 272)	Chain-growth (acrylate/methacrylate) or step-growth thiol–ene (norbornene); control arm number/MW/%, crosslinker stoichiometry <sup>273</sup>	Bio-inert, require adhesion motifs or matrix fragments, enzyme-cleavable links enable cell-driven remodelling <sup>251</sup>	Pros: unrivaled tunability, bio-inert “blank slate”. Cons: lacks all inherent bioactivity, requires extensive functionalization.

fragments because pure PEG is bio-inert. Another important consideration in vascularization is matrix degradation. PEG hydrogels can be functionalized with protease-sensitive peptide crosslinks such as Ac-GCRD-GPQGIWQG-DRCG to enable cell-driven degradation.<sup>259</sup>

Beyond the platforms analyzed above, novel hydrogels such as poly(*N*-isopropylacrylamide) (PNIPAAm) gels and self-assembling peptide (SAP) hydrogels (RADA16 carrying the Ser–Asp–Lys–Pro (SDKP) motif) have been evaluated in cardiac repair. PNIPAAm hydrogels have increased neovascularization and improved function in rat MI models, whereas (RADA)4-SDKP has increased VEGF release from HUVECs and boosted vessel area in chorioallantoic membrane (CAM) assays, with greater microvasculature in infarcted rat hearts.<sup>260–262</sup> While the published studies generally do not vary mechanical properties yet, these materials show promising future directions. Several review papers discuss the variety of synthetic gels available for cardiac repair, injectable, and hydrogel applications in detail (Table 2).<sup>263–265</sup>

## 5. *In vitro* vascular models

Post-MI tissue mechanics provide the target context for *in vitro* vascular models intended for cardiac repair. The passive myocardial Young's modulus in healthy tissue is often reported in

the single-digit to tens of kPa range whereas infarct/fibrotic regions report around 20–100 kPa or higher in large-animal and human assessments, with marked viscoelastic changes during healing. Thus, hydrogel systems tuned from 1–10 kPa to 20–100 kPa allow testing how matrix stiffness/viscoelasticity differentially regulates angiogenesis and inosculature under cardiac-relevant mechanics.<sup>274,275</sup> Moreover, effective vascularization is essential for engineering viable cardiac tissues, especially thick constructs mimicking the myocardium, where diffusion alone cannot sustain cell viability beyond 100–200  $\mu\text{m}$ .<sup>276,277</sup> Perfusable hydrogel models overcome this limitation by incorporating engineered channels or self-assembled networks that enable convective nutrient/waste transport and crucially, allow the study of vascular integration, barrier function, and hemodynamic responses under physiologically relevant conditions.

### 5.1 Bottom-up vascularization

Bottom-up vascularization strategies such as self-assembling networks and modular spheroid assembly rely on the intrinsic ability of endothelial cells to organize into capillary-like structures. In self-assembling systems, ECs are co-cultured with supporting stromal cells (e.g., fibroblasts, pericytes, or mesenchymal stem cells) to recapitulate the native cell–cell crosstalk during vessel formation and stabilize nascent vascu-



lar networks.<sup>278</sup> However, these networks are typically randomly oriented and require integration with microfluidics to sustain perfusion in macroscale constructs.

**5.1.1 Self-assembled EC-stromal networks.** The architecture and function of self-assembled vascular networks are tightly regulated by the hydrogel's physical properties. For example, low-modulus, fast stress-relaxing hydrogels (*e.g.*,  $G' = 500$  Pa) yield wider, more mature, and denser capillary sprouts, while overly stiff or non-relaxing matrices suppress branching and favor static EC morphologies.<sup>129</sup> A physiologic "sweet spot" in matrix mechanics, combining stiffness, viscoelasticity, and controlled degradability, is essential for multicellular invasion and robust, sustained network formation. Micro-architectural features further impact outcomes. Recently, there has been growing interest in granular gels where materials are formed by jamming together microscopic hydrogel particles to create a macroporous, injectable scaffold. The porous nature allows rapid endothelial migration and vessel ingrowth.<sup>129,151,279,280</sup> Similarly, aligned topographies (*e.g.*, *via* microfibre scaffolds) can induce anisotropic vascular orientation.<sup>281,282</sup>

Modular assembly offers an alternative, where pre-vascularized spheroids or microtissues are assembled into larger tissues. These micro-units inosculate post-assembly to form connected networks, preserving cell viability and architectural fidelity, though challenges remain in achieving uniform vascular density and precise organization. Studies show that when embedded in a soft, viscoelastic hydrogel, these modules inosculate and connect both with each other and the host after implantation, accelerating perfusion and functional integration.<sup>283</sup> By contrast, stiffer or non-degradable matrices can isolate spheroids, limiting vascular network formation and integration.<sup>283</sup> *In vivo*, compliant, degradable hydrogels enable organoid- or spheroid-based constructs to form larger, more mature vessels, resulting in superior graft perfusion and improved cardiac function post-MI.<sup>284–286</sup>

**5.1.2 Microfluidic vascular-on-a-chip systems.** Microfluidic organ-on-chip systems can provide precise control over the microenvironment, enabling advanced modelling of perfusable microvessels *in vitro*. These devices typically feature endothelialized microchannels<sup>287,288</sup> fabricated in polymers like polydimethylsiloxane (PDMS), emulating arterioles, venules, or capillaries (Fig. 3A). Under continuous perfusion, they achieve physiological flow regimes and hemodynamic shear forces ( $1\text{--}60$  dyn cm<sup>-2</sup>).<sup>289</sup> These models are crucial because a dynamic environment elicits distinct cellular behaviours such as cell alignment and tight junction changes that are not fully captured in static 2D or 3D cultures (Fig. 3C).<sup>290</sup> Critically, many endothelial behaviours are flow dependent, and thus static vascular models without sustained perfusion can underrepresent vascular biology. For example, networks cultured under static conditions lost perfusion by day 12, whereas continuous perfusion maintained perfusable vessels for at least 51 days and reduced inflammatory signalling.<sup>291</sup> Furthermore, these platforms can facilitate and allow the study of complex intercellular interactions such as those between

endothelial and mural cells, which have a significant impact on tube formation, perfusibility and establishment of microvascular networks (Fig. 3B).<sup>292,293</sup> Finally, vessel-on-chip systems are powerful tools for examining angiogenesis, drug transport, vascular pathology, and disease mechanisms tailored to individuals and specific pathological conditions, by incorporating patient-derived cells and tuning the mechanical properties of specific areas to capture disease- and patient-specific vascular phenotypes and test personalized therapeutic responses in a controlled, perfused microenvironment (Fig. 3D and E).<sup>294,295</sup> Limitations include PDMS absorption of hydrophobic molecules and challenges in scaling tissue integration. To overcome PDMS-related constraints, investigators can utilize photocrosslinkable GelMA systems. By modulating GelMA's degree of methacrylation and increasing the GelMA wt%, the Young's modulus can be tuned up to the tens of kPa.<sup>296–298</sup> Similarly, diacrylated Pluronic F127 hydrogels (15 wt% polymer,  $\geq 90\%$  acrylation) form non-swelling covalent networks ( $G' = 1\text{--}2$  kPa;  $E = 75$  kPa) that preserve channel geometry under flow for a week.<sup>299</sup>

## 5.2 3D bioprinting

3D bioprinting brings together cells and biomaterials in specific architectures to build vascularized tissues layer-by-layer. Bioprinting enables the direct fabrication of channels or vessel-like structures within a tissue construct, providing a patterned vasculature on demand. High-impact advances have shown that bioprinting can produce perfusion-ready vascular networks in thick tissues, addressing the diffusion limit that constrains tissue engineering.

**5.2.1 Sacrificial printing.** Sacrificial bioprinting involves depositing a temporary filament (the fugitive ink) in the pattern of the desired vascular network, and then encasing it with a cell-laden matrix. Subsequently the sacrificial material is removed to leave behind open channels that can be seeded with cells. For example, sacrificial writing into functional tissue (SWIFT) bioprinting prints sacrificial gelatin inks through densely packed organoid matrices to form perfusable channels within centimeter-scale, high-cell-density cardiac patches.<sup>301</sup>

The mechanical characteristics of both the sacrificial ink and support bath are critical. A matrix with insufficient yield stress fails to maintain structure, while excessive stiffness can hinder cell viability and channel fidelity.<sup>302</sup> These trade-offs can be mitigated by adding rheological modifiers. For example, blending LAPONITE® RDS and CaCl<sub>2</sub> into the Pluronic bath raises its yield stress to 47 Pa and confers rapid thixotropic recovery, resulting in high cell viability.<sup>303</sup> Similarly, in ECs embedded within a glucose-sensitive poly(ethylene glycol) diacrylate (PEGDA)/dithiothreitol (DTT)/poly(ethyleneimine) (PEI)-borax ink with tailored stiffness ( $G' = 8.5$  kPa) and self-healing properties, the cells in the ink maintained 79.4% viability post-print, proliferated four-fold over 14 days, and formed capillary-like networks; softer formulations ( $G' < 8.5$  kPa) showed larger filament diameters and were more susceptible to structural collapse due to low modulus and



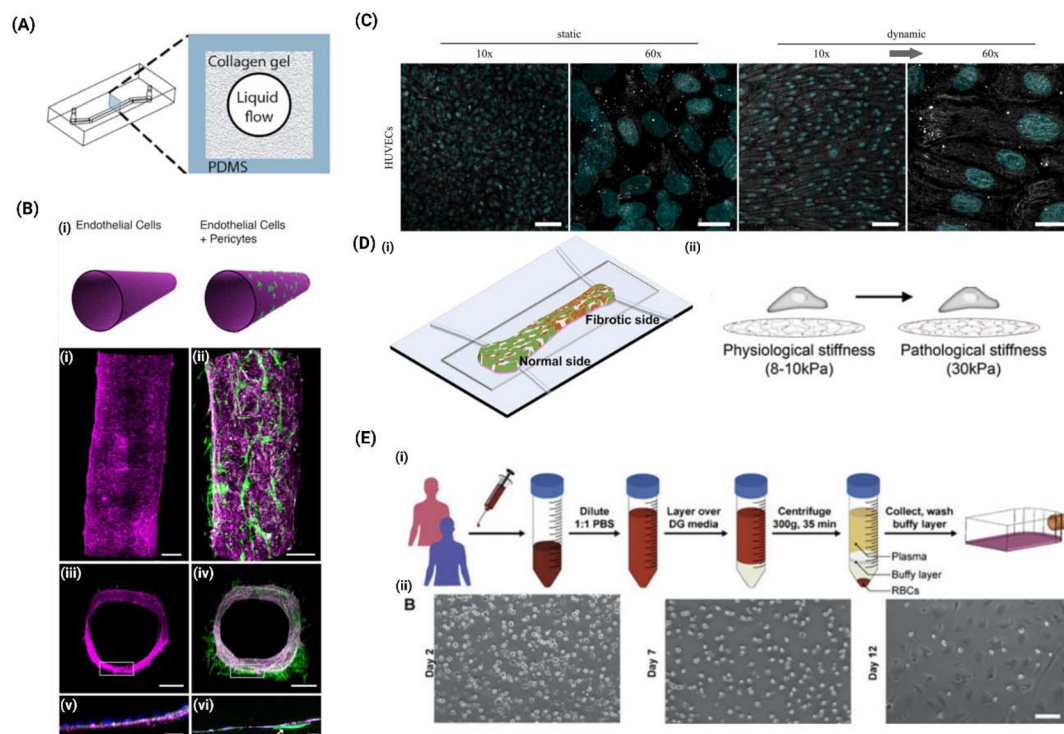


**Fig. 3** Engineered organ-on-chip platforms for vascular and cardiac disease modeling. (A) Schematic diagram of the PDMS vasculature organ on a chip structure used to generate the 3D blood–brain barrier (BBB) chip. (B) Engineered microvessels in a 3D BBB chip: surface (i, ii) cross-sections (iii, iv), and high-magnification cross-section “zoom-ins” of the engineered microvessel wall (v, vi). (A and B) Adapted from ref. 288 (Copyright 2016, Herland *et al.*) and is open access. (C) Confluent HUVECs exposed to homogeneous laminar shear stress ( $\sim 6.6 \text{ dyn cm}^{-2}$ ) in a parallel-plate flow chamber progressively elongate and align in the direction of flow, whereas static cultures remain largely non-oriented. Adapted from ref. 290 (Copyright 2022, Lindner *et al.*) and is open access. (D) (i) Schematics of a heteropolar scar myocardium organ-on-chip model that spatially compares stiff fibrotic scar and healthy cardiac tissues to recapitulate the regional heterogeneity of a focal scar, border zone, and adjacent myocardium, enabling the study of regional remodelling and differential drug responses. (ii) Schematic comparing the mechanical microenvironment used to model the healthy myocardium vs fibrotic scar, showing a shift from physiological stiffness ( $\sim 8\text{--}10 \text{ kPa}$ ) to pathological stiffness ( $\sim 30 \text{ kPa}$ ). Adapted from ref. 300 with permission from the Royal Society of Chemistry, copyright 2019. (E) (i) Cell isolation workflow for patient cell isolation for personalized drug-response testing; (ii) removal of non-adherent leukocytes and platelets from culture flasks seeded with cells isolated from the buffy layer. (D) and (E) Adapted from ref. 294 with permission from the Royal Society of Chemistry, copyright 2019.

poor stackability, whereas a slightly stiffer control hydrogel ( $G' = 10 \text{ kPa}$ ) was more brittle and harder to inject as continuous filaments.<sup>304</sup> More recently, shear-thinning PEG–norbornene granular slurries were used as support baths for the sacrificial patterning of mesoscale channels while preserving subsequent interstitial microvascular self-assembly in  $>500 \text{ mm}^3$  constructs.<sup>305</sup> While sacrificial printing is well suited for building perfusable channels ranging from  $115 \mu\text{m}$  up to millimetres in diameter, its resolution is limited mainly by nozzle size and printing fidelity and offers limited precision at the capillary scale.

### 5.2.2 Digital and stereolithography printing.

Stereolithographic bioprinting leverages patterned ultraviolet (UV) or visible light to photopolymerize bio-resins into 3D structures with microscale resolution, enabling the creation of intricate vascular networks with high complexity. Techniques like digital light projection polymerize bioinks layer-by-layer, while volumetric printing solidifies the entire structure at once, enabling the rapid fabrication of intricate channels within minutes. Grigoryan *et al.*, for example, used digital

light processing (DLP) stereolithography to fabricate multi-scale hierarchical vascular networks and nested lumens by photopolymerizing bioink using flashing patterned light.<sup>306</sup> The printed channels enabled the formation of functional endothelialized vasculature that supported flow, and related stereolithographic systems have achieved printed feature sizes as small as  $50 \mu\text{m}$ . Unlike extrusion methods, DLP imposes minimal shear stress on cells, and light-based curing enables rapid production of complex 3D constructs. In addition, DLP systems now allow stiffness tuning by adjusting polymer concentration or mixing ratios. For example, Wang *et al.* decreased PEG content in a PEG/GelMA ink to reduce the compressive Young's modulus from  $200 \text{ kPa}$  to  $20 \text{ kPa}$ , which improved cell viability and facilitated EC spreading through enlarged pores.<sup>307</sup>

Volumetric printing extends stereolithographic principles by curing entire 3D constructs at once using a patterned light source, such as holographic or tomographic projection. For example, holographic or tomographic techniques can print a complete network within tens of seconds.<sup>308,309</sup> The major



upside of stereolithography is its high resolution and geometric fidelity as one can replicate anatomically realistic branching angles, vessel tortuosity, and hierarchical vascular geometries across multiple size scales by appropriate mask designs.<sup>310–312</sup> Moreover, light-based printing is contactless, reducing shear stresses on cells that come with extrusion methods.<sup>311</sup> The downsides relate to materials and biocompatibility. Photoinitiators and monomers required for cross-linking can be cytotoxic if not carefully chosen; thus, bioinks must be formulated to balance printability with cell toxicity. Additionally, most stereolithography printers work with synthetic polymer solutions (e.g. PEG-diacrylate, GelMA) that have lower cell content than extrusion bioinks, and thus encapsulated cells are often present but at moderate densities due to light scattering constraints. Post-print cell seeding is usually needed to line the channels with endothelium.

**5.2.3 Coaxial printing.** Coaxial bioprinting employs concentric nozzles to simultaneously extrude a core and a shell material, forming hollow, tubular vessels in a single step. An inner needle delivers a core material or crosslinker, while an outer needle deposits a cell-laden hydrogel; the hydrogel solidifies around the core, forming a continuous lumen.<sup>313,314</sup>

This method produces channels with tunable diameters ranging from 100  $\mu\text{m}$  to 1 mm and allows the spatial organization of cells into multi-layered vessel walls, mimicking native vessels (Fig. 4A–E).<sup>313–317</sup> For example, an indirect co-culture places an endothelial-cell bioink in the core and an osteogenic-cell bioink in the shell to model vascularized osteogenic tissue and probe endothelial osteogenic interactions, with confocal imaging confirming a core-shell arrangement at printed junctions along a branched structure (Fig. 4F–H).<sup>318</sup>

The mechanical properties of the printed constructs can directly influence the cellular responses. For instance, Gao *et al.* doubled the alginate content from 2 wt% to 4 wt% which increased the tensile strength and decreased the likelihood of filament fusion.<sup>319</sup> The printed hollow, perfusable filament maintained higher cell viability (67%), whereas non-perfusible slabs of the same composition supported only 50% viable cells by day 7,<sup>320</sup> illustrating that perfusion through the channel supports mass transport. In nanoclay/*N*-acryloyl glycinamide (NAGA)/GelMA biohybrid vessels, modulation of the NAGA:GelMA ratio enabled control over the stiffness and burst pressure: HUVEC proliferation peaked on intermediate-stiffness gels (7 : 3 ratio), while endothelial markers (CD31, von

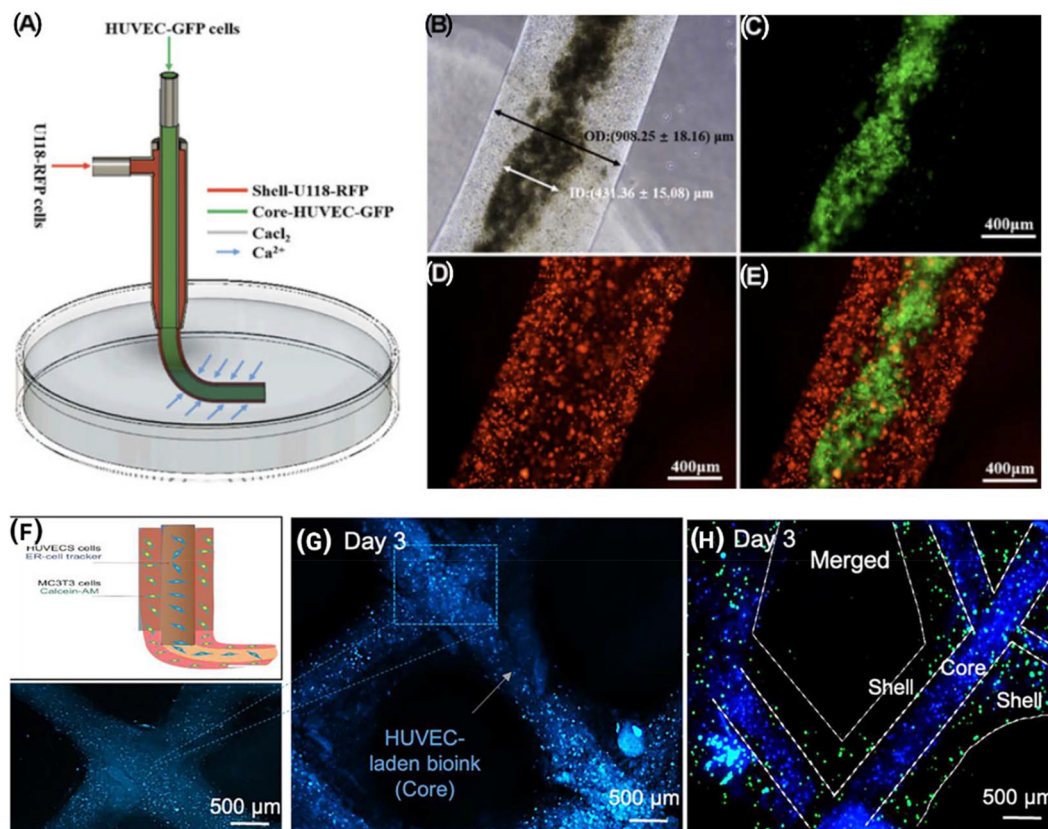


**Fig. 4** Coaxial bioprinting strategies for spatially organized multicellular constructs. (A) Schematic of a coaxial print that places endothelial cells in the core (green) and companion cells in the shell (red). (B) Bright-field view of the printed fibre. (C) Green channel: cells confined to the core. (D) Red channel: cells localized to the shell. (E) Merge confirming the concentric shell-core architecture. (A–E) Adapted from ref. 317 (Copyright 2021, Wang *et al.*) and is open access. (F) Schematic of the indirect co-culture: endothelial-cell bioink in the core and osteogenic-cell bioink in the shell. (G) Low-magnification confocal image shows the printed junction with core (endothelial, blue) surrounded by shell (osteogenic, green). (H) Merged view tracing the core-shell boundaries along the branched structure. (F–H) Adapted from ref. 318 with permission from Wiley, copyright 2022.



Willebrand factor (vWF)) maximized on softer formulations (5:5 ratio), indicating a stiffness-dependent regulation of endothelial phenotype.<sup>321</sup> Similarly, triple-coaxial grafts with reduced alginate (0.5% w/v) in the smooth muscle layer lowered stiffness sufficiently to restore human aortic smooth muscle cells (HAoSMC) spreading and boosted differentiation markers ( $\alpha$ -smooth muscle actin, smooth muscle protein 22- $\alpha$ ), while the endothelial core (3% vascular ECM) achieved 96% luminal coverage and maintained 21-day patency *in vivo*, confirming that targeted softening accelerates tissue maturation without compromising mechanical integrity.<sup>320</sup> However, while capable of producing implantable-scale grafts and microfluidic networks, coaxial printing faces challenges with nozzle clogging, extrusion consistency, diameter control, and limited geometric complexity for features like high branching. It excels for generating larger, continuous conduits but struggles at capillary scales.

## 6. Discussion and conclusion

Mechanical cues within the cardiac ECM, such as stiffness, viscoelasticity, degradability, porosity, and anisotropy, significantly affect EC behaviours and vascularization.

Recent advances in biomaterial engineering, particularly hydrogels with independently tunable mechanical properties, have allowed researchers to more systematically investigate how individual matrix features regulate neovascularization and tissue remodelling. For example, stress relaxation can be tuned independently of stiffness by incorporating dynamic covalent or supramolecular bonds into a stable network, or by directly altering the molecular structure of the crosslinks, such as changing the type of bond by selecting between aliphatic aldehydes and aromatic benzaldehydes to form hydrazone networks.<sup>129,322</sup> Interpenetrating polymer networks provide another approach. Combining an inert mechanical backbone with a bioactive component provides structural reinforcement, increasing the overall stiffness without requiring gel densification that compromises pore architecture.<sup>125,323</sup> However, isolating the effects of single mechanical cues remains challenging, because while experimental designs typically decouple two target variables, they often inadvertently alter confounding factors such as porosity, plasticity, anisotropy, and essential biological cues, eliciting divergent endothelial behaviours even with similar mechanical properties due to differences in biochemical composition and biochemical signalling. For instance, in PEG hydrogels, endothelial network formation can differ at a comparable stiffness depending on how the modulus is achieved, reflecting material-specific microenvironmental differences beyond bulk mechanics.<sup>324</sup> Similarly, phenol-functionalized gelatin hydrogels only supported HUVEC network formation when blended with hyaluronic acid, whereas gelatin alone or gelatin–alginate blends with a comparable Young's modulus did not.<sup>325</sup>

Further refinement of hydrogel platforms is needed to more accurately recapitulate the dynamic, hierarchical, and spatially

heterogeneous nature of native myocardium. This includes mimicking temporal changes in stiffness and viscoelasticity during healing, spatial gradients in porosity and ligand presentation, and multi-scale anisotropy of fibre organization. Because material, mechanical, and biochemical signals interact in complex ways, there is currently no universal standard for defining an “optimal” range of mechanical properties for vascularization.

These challenges are compounded by an incomplete understanding of the mechanics and matrix composition of healthy human cardiac tissue, which is rarely accessible for direct study. Moving forward, there is a need to engineer matrices that support not only robust but also spatially organized directional vascularization, mimicking the anisotropic and hierarchical structure of native myocardium. While *in vitro* models have yielded valuable insights, integrating hydrogel design with spatiotemporally controlled biochemical and mechanical cues, patient-specific cells and perfusion systems will be essential. Finally, translating these designs *in vivo* presents cross-cutting challenges. Tissue remodelling presents a complex and evolving environment, complicating the attribution of vascular outcomes to specific mechanical cues. Furthermore, how injected or implanted hydrogels interact with and alter the local tissue mechanical environment *in situ* remains incompletely understood. Rigorous *in vivo* evaluation of vascular integration, perfusion, and functional outcomes will be needed to bridge the gap between engineered tissue constructs and clinically meaningful myocardial repair.

## Conflicts of interest

There are no conflicts to declare.

## Data availability

No primary research results, software or code have been included and no new data were generated or analysed as part of this review.

## Acknowledgements

This study was supported by NSERC Discovery Grant (RGPIN-2025-06790) and St Paul's foundation.

## References

- 1 M. Di Cesare, H. Bixby, T. Gaziano, L. Hadeed, C. Kabudula, D. V. McGhie, J. Mwangi, B. Pervan, P. Perel, D. Piñeiro, S. Taylor and F. Pinto, World Heart Report 2023 Confronting The World's Number One Killer, World Heart Federation, 2023.
- 2 P. Christia and N. G. Frangogiannis, *Eur. J. Clin. Invest.*, 2013, **43**, 986–995.



- 3 A. Yabluchanskiy, R. J. Chilton and M. L. Lindsey, *Congestive Heart Failure*, 2013, **19**, E5–E8.
- 4 K. van der Heiden, B. J. Krenning, D. Merkus and M. R. Bernsen, in *Imaging of Inflammation and Infection in Cardiovascular Diseases*, ed. F. Caobelli, Springer International Publishing, Cham, 2021, ch. 5, pp. 109–159, DOI: [10.1007/978-3-030-81131-0\\_5](https://doi.org/10.1007/978-3-030-81131-0_5).
- 5 Z. Mallat and A. Tedgui, *Br. J. Pharmacol.*, 2000, **130**, 947–962.
- 6 W. Risau, *Nature*, 1997, **386**, 671–674.
- 7 D. Hanjaya-Putra, K. T. Wong, K. Hirotsu, S. Khetan, J. A. Burdick and S. Gerecht, *Biomaterials*, 2012, **33**, 6123–6131.
- 8 P. Vempati, A. S. Popel and F. Mac Gabhann, *Cytokine Growth Factor Rev.*, 2014, **25**, 1–19.
- 9 I. Andreu, T. Luque, A. Sancho, B. Pelacho, O. Iglesias-Garcia, E. Melo, R. Farre, F. Prosper, M. R. Elizalde and D. Navajas, *Acta Biomater.*, 2014, **10**, 3235–3242.
- 10 A. Alonso, A. Ebben and M. Dabagh, *Biomech. Model. Mechanobiol.*, 2023, **22**, 1919–1933.
- 11 T. Liang, J. Liu, F. Liu, X. Su, X. Li, J. Zeng, F. Chen, H. Wen, Y. Chen, J. Tao, Q. Lei, G. Li and P. Cheng, *ACS Omega*, 2024, **9**, 37505–37529.
- 12 H. E. Mewhort, J. D. Turnbull, H. C. Meijndert, J. M. Ngu and P. W. Fedak, *J. Thorac. Cardiovasc. Surg.*, 2014, **147**, 1650–1659.
- 13 H. E. Mewhort, J. D. Turnbull, A. Satriano, K. Chow, J. A. Flewitt, A. C. Andrei, D. G. Guzzardi, D. A. Svystonyuk, J. A. White and P. W. Fedak, *J. Heart Lung Transplant.*, 2016, **35**, 661–670.
- 14 M. L. Lindsey, J. Gannon, M. Aikawa, F. J. Schoen, E. Rabkin, L. Lopresti-Morrow, J. Crawford, S. Black, P. Libby, P. G. Mitchell and R. T. Lee, *Circulation*, 2002, **105**, 753–758.
- 15 Y. Tan, M. Li, X. Ma, D. Shi and W. Liu, *Front. Cardiovasc. Med.*, 2025, **12**, 1426583.
- 16 T. Matsunaga, D. C. Warltier, J. Tessmer, D. Weihrauch, M. Simons and W. M. Chilian, *Am. J. Physiol. Heart Circ. Physiol.*, 2003, **285**, H352–H358.
- 17 D. S. Figueroa, S. F. Kemeny and A. M. Clyne, *J. Biomech. Eng.*, 2014, **136**, 101010.
- 18 S. Koudstaal, S. J. Jansen of Lorkeers, F. J. van Slochteren, T. I. van der Spoel, T. P. van de Hoef, J. P. Sluijter, M. Siebes, P. A. Doevendans, J. J. Piek and S. A. Chamuleau, *J. Cell. Mol. Med.*, 2013, **17**, 1128–1135.
- 19 R. Karch, F. Neumann, R. Ullrich, J. Neumuller, B. K. Podesser, M. Neumann and W. Schreiner, *Cardiovasc. Pathol.*, 2005, **14**, 135–144.
- 20 M. R. Mehrabi, N. Serbecic, F. Tamaddon, C. Kaun, K. Huber, R. Pacher, T. Wild, G. Mall, J. Wojta and H. D. Glogar, *Cardiovasc. Res.*, 2002, **56**, 214–224.
- 21 D. J. Campbell, J. B. Somaratne, A. J. Jenkins, D. L. Prior, M. Yui, J. F. Kenny, A. E. Newcomb, D. J. Kelly and M. J. Black, *Int. J. Cardiol.*, 2013, **167**, 1027–1037.
- 22 P. Gkontra, K. A. Norton, M. M. Zak, C. Clemente, J. Aguero, B. Ibanez, A. Santos, A. S. Popel and A. G. Arroyo, *Sci. Rep.*, 2018, **8**, 1854.
- 23 S. A. Leanca, D. Crisu, A. O. Petris, I. Afrasanie, A. Genes, A. D. Costache, D. N. Tesloianu and I. I. Costache, *Life*, 2022, **12**, 1111.
- 24 W. Chan, S. J. Duffy, D. A. White, X. M. Gao, X. J. Du, A. H. Ellims, A. M. Dart and A. J. Taylor, *JACC Cardiovasc. Imaging*, 2012, **5**, 884–893.
- 25 L. Galiuto, F. A. Gabrielli, A. Lombardo, G. La Torre, A. Scara, A. G. Rebuzzi and F. Crea, *Heart*, 2007, **93**, 565–571.
- 26 N. G. Frangogiannis, *J. Clin. Invest.*, 2017, **127**, 1600–1612.
- 27 C. Leclech, C. F. Natale and A. I. Barakat, *J. Cell Sci.*, 2020, **133**, jcs239889.
- 28 A. Nikolov and N. Popovski, *Metabolites*, 2022, **12**, 297.
- 29 J. E. Bishop, R. Greenbaum, D. G. Gibson, M. Yacoub and G. J. Laurent, *J. Mol. Cell Cardiol.*, 1990, **22**, 1157–1165.
- 30 M. Eghbali and K. T. Weber, *Ann. N. Y. Acad. Sci.*, 2006, **580**, 468–472.
- 31 G. M. Fomovsky, S. Thomopoulos and J. W. Holmes, *J. Mol. Cell Cardiol.*, 2010, **48**, 490–496.
- 32 D. Singh, V. Rai and D. K. Agrawal, *Cardiol. Cardiovasc. Med.*, 2023, **7**, 5–16.
- 33 L. Alex, I. Tuleta, S. C. Hernandez, A. Hanna, H. Venugopal, M. Astorkia, C. Humeres, A. Kubota, K. Su, D. Zheng and N. G. Frangogiannis, *Circulation*, 2023, **148**, 882–898.
- 34 M. Wang, K. R. McGraw, R. E. Monticone and G. Pintus, *Biomolecules*, 2025, **15**, 153.
- 35 P. Mohindra, J. X. Zhong, Q. Fang, D. L. Cuylear, C. Huynh, H. Qiu, D. Gao, B. N. Kharbikar, X. Huang, M. L. Springer, R. J. Lee and T. A. Desai, *NPJ Regen. Med.*, 2023, **8**, 60.
- 36 D. Westermann, J. Mersmann, A. Melchior, T. Freudenberger, C. Petrik, L. Schaefer, R. Lullmann-Rauch, O. Lettau, C. Jacoby, J. Schrader, S. M. Brand-Herrmann, M. F. Young, H. P. Schultheiss, B. Levkau, H. A. Baba, T. Unger, K. Zacharowski, C. Tschope and J. W. Fischer, *Circulation*, 2008, **117**, 1269–1276.
- 37 E. L. George, E. N. Georges-Labouesse, R. S. Patel-King, H. Rayburn and R. O. Hynes, *Development*, 1993, **119**, 1079–1091.
- 38 J. Song, X. Zhang, K. Buscher, Y. Wang, H. Wang, J. Di Russo, L. Li, S. Lutke-Enking, A. Zarbock, A. Stadtmann, P. Striewski, B. Wirth, I. Kuzmanov, H. Wiendl, D. Schulte, D. Vestweber and L. Sorokin, *Cell Rep.*, 2017, **18**, 1256–1269.
- 39 H. Yang, T. K. Borg, Z. Wang, Z. Ma and B. Z. Gao, *Ann. Biomed. Eng.*, 2014, **42**, 1148–1157.
- 40 J. Lim, D. R. Machin, A. J. Donato and A. Z. Chignalia, in *Current Topics in Membranes*, ed. I. S. Fancher, Academic Press, 2023, vol. 91, pp. 139–156.
- 41 D. T. Little, C. M. Howard, E. Pendergraft, K. R. Brittan, T. N. Audam, E. W. Lukudu, J. Smith, D. Nguyen, Y. Nishida, Y. Yamaguchi, R. E. Brainard, R. A. Singhal



- and S. P. Jones, *Am. J. Physiol. Cell Physiol.*, 2025, **328**, C939–C953.
- 42 M. Rusu, K. Hilse, A. Schuh, L. Martin, I. Slabu, C. Stoppe and E. A. Liehn, *Sci. Rep.*, 2019, **9**, 16744.
- 43 J. P. Cleutjens, M. J. Verluyten, J. F. Smiths and M. J. Daemen, *Am. J. Pathol.*, 1995, **147**, 325–338.
- 44 S. P. Arunachalam, A. Arani, F. Baffour, J. A. Rysavy, P. J. Rossman, K. J. Glaser, D. S. Lake, J. D. Trzasko, A. Manduca, K. P. McGee, R. L. Ehman and P. A. Araoz, *Magn. Reson. Med.*, 2018, **79**, 361–369.
- 45 C. T. Stoeck, C. von Deuster, M. Fuetterer, M. Polacin, C. F. Waschkies, R. J. H. van Gorkum, M. Kron, T. Fleischmann, N. Cesarovic, M. Weisskopf and S. Kozerke, *J. Cardiovasc. Magn. Reson.*, 2021, **23**, 103.
- 46 P. Gkontra, K.-A. Norton, M. M. Žak, C. Clemente, J. Agüero, B. Ibáñez, A. Santos, A. S. Popel and A. G. Arroyo, *Sci. Rep.*, 2018, **8**, 1854.
- 47 B. S. Burlew and K. T. Weber, *Herz*, 2002, **27**, 92–98.
- 48 J. J. Thune and S. D. Solomon, *Curr. Heart Fail. Rep.*, 2006, **3**, 170–174.
- 49 P. Piątek-Matuszak, R. Paślowski, U. Paśławska, L. Kiczak, M. Płóciennik, A. Janiszewski, M. Michałek, A. Gwizdała, J. Kaźmierczak and J. Gorący, *J. Clin. Med.*, 2022, **11**, 5430.
- 50 B. I. Jugdutt, in *Cardiac Remodeling: Molecular Mechanisms*, ed. B. I. Jugdutt and N. S. Dhalla, Springer, New York, NY, 2013, pp. 525–545.
- 51 A. A. Sovari, A. Shroff and A. G. Kocheril, *Expert Rev. Cardiovasc. Ther.*, 2012, **10**, 267–270.
- 52 M. Dobaczewski, C. Gonzalez-Quesada and N. G. Frangogiannis, *J. Mol. Cell. Cardiol.*, 2010, **48**, 504–511.
- 53 S. D. Zimmerman, D. P. Thomas, S. G. Velleman, X. Li, T. R. Hansen and R. J. McCormick, *Am. J. Physiol. Heart Circ. Physiol.*, 2001, **281**, H1816–H1822.
- 54 P. Contessotto, R. Spelat, F. Ferro, V. Vysockas, A. Krivickiene, C. Jin, S. Chantepie, C. Chinello, A. G. Pauza, C. Valente, M. Rackauskas, A. Casara, V. Zigmantaite, F. Magni, D. Papy-Garcia, N. G. Karlsson, E. Ereminiene, A. Pandit and M. Da Costa, *Nat. Commun.*, 2023, **14**, 995.
- 55 Y. Yu, G. Yin, S. Bao and Z. Guo, *Mol. Med. Rep.*, 2018, **17**, 3519–3526.
- 56 G. Narayanan, A. Halim, A. Hu, K. G. Avin, T. Lu, D. Zehnder, T. Hato, N. X. Chen, S. M. Moe and K. Lim, *Kidney360*, 2023, **4**, 1562–1579.
- 57 B. I. Jugdutt, M. J. Joljart and M. I. Khan, *Circulation*, 1996, **94**, 94–101.
- 58 J. M. Wainwright, C. A. Czajka, U. B. Patel, D. O. Freytes, K. Tobita, T. W. Gilbert and S. F. Badylak, *Tissue Eng. Part C. Methods*, 2010, **16**, 525–532.
- 59 M. M. Ulrich, A. M. Janssen, M. J. Daemen, L. Rappaport, J. L. Samuel, F. Contard, J. F. Smits and J. P. Cleutjens, *J. Mol. Cell Cardiol.*, 1997, **29**, 2533–2543.
- 60 B. V. Shekhonin, S. B. Guriev, S. B. Irgashev and V. E. Koteliansky, *J. Mol. Cell Cardiol.*, 1990, **22**, 533–541.
- 61 A. A. Knowlton, C. M. Connelly, G. M. Romo, W. Mamuya, C. S. Apstein and P. Brecher, *J. Clin. Invest.*, 1992, **89**, 1060–1068.
- 62 C. Urbich, E. Dernbach, A. Reissner, M. Vasa, A. M. Zeiher and S. Dimmeler, *Arterioscler., Thromb., Vasc. Biol.*, 2002, **22**, 69–75.
- 63 A. Hielscher, K. Ellis, C. Qiu, J. Porterfield and S. Gerecht, *PLoS One*, 2016, **11**, e0147600.
- 64 A. M. Schor, I. Ellis and S. L. Schor, *Methods Mol. Med.*, 2001, **46**, 163–183.
- 65 J. M. Wells, A. Gaggar and J. E. Blalock, *Matrix Biol.*, 2015, **44–46**, 122–129.
- 66 Y. Hamano, M. Zeisberg, H. Sugimoto, J. C. Lively, Y. Maeshima, C. Yang, R. O. Hynes, Z. Werb, A. Sudhakar and R. Kalluri, *Cancer Cell*, 2003, **3**, 589–601.
- 67 M. Sokolowska, L. Y. Chen, M. Eberlein, A. Martinez-Anton, Y. Liu, S. Alsaaty, H. Y. Qi, C. Logun, M. Horton and J. H. Shelhamer, *J. Biol. Chem.*, 2014, **289**, 4470–4488.
- 68 C. C. Termeer, P. Prehm and J. C. Simon, in *Hyaluronan*, Elsevier, 2002, pp. 457–468, DOI: [10.1533/9781845693121.457](https://doi.org/10.1533/9781845693121.457).
- 69 R. Krasinski and H. Tchorzewski, *Postepy Hig. Med. Dosw.*, 2007, **61**, 683–689.
- 70 N. G. Frangogiannis, *Physiol. Rev.*, 2012, **92**, 635–688.
- 71 M. F. Berry, A. J. Engler, Y. J. Woo, T. J. Pirolli, L. T. Bish, V. Jayasankar, K. J. Morine, T. J. Gardner, D. E. Discher and H. L. Sweeney, *Am. J. Physiol. Heart Circ. Physiol.*, 2006, **290**, H2196–H2203.
- 72 F. Villarreal, J. Omens, W. Dillmann, J. Risteli, J. Nguyen and J. Covell, *J. Mol. Cell Cardiol.*, 2004, **36**, 597–601.
- 73 P. Y. Cheung, G. Sawicki, M. Wozniak, W. Wang, M. W. Radomski and R. Schulz, *Circulation*, 2000, **101**, 1833–1839.
- 74 R. Esipov, K. Beyrakhova, V. Likhvantseva, E. Stepanova, V. Stepanenko, M. Kostromina, Y. Abramchik and A. Miroshnikov, *Biochimie*, 2012, **94**, 1368–1375.
- 75 A. Chandrabhatla, *Using a Computational Model of Cardiac Fibroblast Signaling to Screen for Drugs Effective Against Heart Failure*, University of Virginia, 2017.
- 76 J. E. Murphy-Ullrich, *J. Clin. Invest.*, 2001, **107**, 785–790.
- 77 W. Chen and N. G. Frangogiannis, *Biochim. Biophys. Acta, Mol. Cell Res.*, 2013, **1833**, 945–953.
- 78 F. Bordeleau, B. N. Mason, E. M. Lollis, M. Mazzola, M. R. Zanotelli, S. Somasegar, J. P. Califano, C. Montague, D. J. LaValley, J. Huynh, N. Mencia-Trinchant, Y. L. Negrón Abril, D. C. Hassane, L. J. Bonassar, J. T. Butcher, R. S. Weiss and C. A. Reinhart-King, *Proc. Natl. Acad. Sci. U. S. A.*, 2017, **114**, 492–497.
- 79 A. Gorska and A. J. Mazur, *Cell. Mol. Life Sci.*, 2022, **79**, 100.
- 80 Y. Guo, F. Mei, Y. Huang, S. Ma, Y. Wei, X. Zhang, M. Xu, Y. He, B. C. Heng, L. Chen and X. Deng, *Bioact. Mater.*, 2022, **7**, 364–376.
- 81 O. Chaudhuri, L. Gu, M. Darnell, D. Klumpers, S. A. Bencherif, J. C. Weaver, N. Huebsch and D. J. Mooney, *Nat. Commun.*, 2015, **6**, 6364.



- 82 N. Daneshjou, N. Sieracki, G. P. van Nieuw Amerongen, D. E. Conway, M. A. Schwartz, Y. A. Komarova and A. B. Malik, *J. Cell Biol.*, 2015, **208**, 23–32.
- 83 B. Piersma, R. A. Bank and M. Boersema, *Front. Med.*, 2015, **2**, 59.
- 84 S. Dupont, L. Morsut, M. Aragona, E. Enzo, S. Giullitti, M. Cordenonsi, F. Zanconato, J. Le Digabel, M. Forcato, S. Bicciato, N. Elvassore and S. Piccolo, *Nature*, 2011, **474**, 179–183.
- 85 N. G. Kim and B. M. Gumbiner, *J. Cell Biol.*, 2015, **210**, 503–515.
- 86 G. Nardone, J. Oliver-De La Cruz, J. Vrbsky, C. Martini, J. Pribyl, P. Skladal, M. Pesl, G. Caluori, S. Pagliari, F. Martino, Z. Maceckova, M. Hajduch, A. Sanz-Garcia, N. M. Pugno, G. B. Stokin and G. Forte, *Nat. Commun.*, 2017, **8**, 15321.
- 87 C. A. Franco, J. Blanc, A. Parlakian, R. Blanco, I. M. Aspalter, N. Kazakova, N. Diguët, E. Mylonas, J. Gao-Li, A. Vaahtokari, V. Penard-Lacronique, M. Fruttiger, I. Rosewell, M. Mericskay, H. Gerhardt and Z. Li, *Development*, 2013, **140**, 2321–2333.
- 88 R. Hinkel, T. Trenkwalder, B. Petersen, W. Husada, F. Gesenhues, S. Lee, E. Hannappel, I. Bock-Marquette, D. Theisen, L. Leitner, P. Boekstegers, C. Cierniewski, O. J. Muller, F. le Noble, R. H. Adams, C. Weinl, A. Nordheim, B. Reichart, C. Weber, E. Olson, G. Posern, E. Deindl, H. Niemann and C. Kupatt, *Nat. Commun.*, 2014, **5**, 3970.
- 89 C. Weinl, H. Riehle, D. Park, C. Stritt, S. Beck, G. Huber, H. Wolburg, E. N. Olson, M. W. Seeliger, R. H. Adams and A. Nordheim, *J. Clin. Invest.*, 2013, **123**, 2193–2206.
- 90 D. Jetta, T. Shireen and S. Z. Hua, *Front. Cell Dev. Biol.*, 2023, **11**, 1198109.
- 91 B. Coste, J. Mathur, M. Schmidt, T. J. Earley, S. Ranade, M. J. Petrus, A. E. Dubin and A. Patapoutian, *Science*, 2010, **330**, 55–60.
- 92 C. Verkest and S. G. Lechner, *Curr. Opin. Physiol.*, 2023, **31**, 100625.
- 93 C. Wang, S. Luo, Y. Yan, J. Li, W. Niu, T. Hong, K. Hao, X. Sun, J. Liu, R. An and J. Li, *Mol. Med.*, 2025, **31**, 147.
- 94 J. Li, B. Hou, S. Tumova, K. Muraki, A. Bruns, M. J. Ludlow, A. Sedo, A. J. Hyman, L. McKeown, R. S. Young, N. Y. Yuldasheva, Y. Majeed, L. A. Wilson, B. Rode, M. A. Bailey, H. R. Kim, Z. Fu, D. A. Carter, J. Bilton, H. Imrie, P. Ajuh, T. N. Dear, R. M. Cubbon, M. T. Kearney, R. K. Prasad, P. C. Evans, J. F. Ainscough and D. J. Beech, *Nature*, 2014, **515**, 279–282.
- 95 Y. Sun, M. Li, G. Liu, X. Zhang, L. Zhi, J. Zhao and G. Wang, *J. Cancer Res. Clin. Oncol.*, 2020, **146**, 1139–1152.
- 96 X. Wang, G. Cheng, Y. Miao, F. Qiu, L. Bai, Z. Gao, Y. Huang, L. Dong, X. Niu, X. Wang, Y. Li, H. Tang, Y. Xu and X. Song, *J. Cell. Mol. Med.*, 2021, **25**, 2238–2253.
- 97 J. Du, P. Liu, Y. Zhou, S. Misener, I. Sharma, P. Leeaw, B. R. Thomson, J. Jin and S. E. Quaggin, *Br. J. Pharmacol.*, 2024, **181**, 4714–4732.
- 98 A. Hooglugt, M. M. van der Stoel, R. A. Boon and S. Huvneers, *Front. Oncol.*, 2020, **10**, 612802.
- 99 M. Hauke, R. Eckenstaler, A. Ripperger, A. Ender, H. Braun and R. A. Benndorf, *J. Am. Heart Assoc.*, 2022, **11**, e025119.
- 100 W. Wang, E. M. Lollis, F. Bordeleau and C. A. Reinhart-King, *FASEB J.*, 2019, **33**, 1199–1208.
- 101 R. Schnellmann, D. Ntekoumes, M. I. Choudhury, S. Sun, Z. Wei and S. Gerecht, *Adv. Sci.*, 2022, **9**, 2201483.
- 102 A. Husain, A. Khadka, A. Ehrlicher, M. Saint-Geniez and R. Krishnan, *Biochem. Biophys. Res. Commun.*, 2022, **586**, 27–33.
- 103 D. J. LaValley, M. R. Zanotelli, F. Bordeleau, W. Wang, S. C. Schwager and C. A. Reinhart-King, *Convergent Sci. Phys. Oncol.*, 2017, **3**, 044001.
- 104 D. Hanjaya-Putra, J. Yee, D. Ceci, R. Truitt, D. Yee and S. Gerecht, *J. Cell. Mol. Med.*, 2010, **14**, 2436–2447.
- 105 J. Karar and A. Maity, *Front. Mol. Neurosci.*, 2011, **4**, 51.
- 106 B. M. Baker and C. S. Chen, *J. Cell Sci.*, 2012, **125**, 3015–3024.
- 107 A. Saraswathibhatla, D. Indana and O. Chaudhuri, *Nat. Rev. Mol. Cell Biol.*, 2023, **24**, 495–516.
- 108 B. Trappmann, J. E. Gautrot, J. T. Connelly, D. G. T. Strange, Y. Li, M. L. Oyen, M. A. Cohen Stuart, H. Boehm, B. Li, V. Vogel, J. P. Spatz, F. M. Watt and W. T. S. Huck, *Nat. Mater.*, 2012, **11**, 642–649.
- 109 B. N. Mason, A. Starchenko, R. M. Williams, L. J. Bonassar and C. A. Reinhart-King, *Acta Biomater.*, 2013, **9**, 4635–4644.
- 110 A. D. Doyle, N. Carvajal, A. Jin, K. Matsumoto and K. M. Yamada, *Nat. Commun.*, 2015, **6**, 8720.
- 111 T. L. Haas, S. J. Davis and J. A. Madri, *J. Biol. Chem.*, 1998, **273**, 3604–3610.
- 112 A. N. Stratman, W. B. Saunders, A. Sacharidou, W. Koh, K. E. Fisher, D. C. Zawieja, M. J. Davis and G. E. Davis, *Blood*, 2009, **114**, 237–247.
- 113 J. Rapp, J. Ness, J. Wolf, A. Hospach, P. Liang, M. J. Hug, H. Agostini, G. Schlunck, C. Lange and F. Bucher, *Biochim. Biophys. Acta, Mol. Basis Dis.*, 2024, **1870**, 167028.
- 114 G. Brusatin, T. Panciera, A. Gandin, A. Citron and S. Piccolo, *Nat. Mater.*, 2018, **17**, 1063–1075.
- 115 S. Dupont, *Exp. Cell Res.*, 2016, **343**, 42–53.
- 116 S. K. Nair, S. Basu, B. Sen, M. H. Lin, A. N. Kumar, Y. Yuan, P. J. Cullen and D. Sarkar, *Sci. Rep.*, 2019, **9**, 1072.
- 117 A. Lesman, D. Rosenfeld, S. Landau and S. Levenberg, *Adv. Drug Delivery Rev.*, 2016, **96**, 176–182.
- 118 G. J. Pahapale, J. Tao, M. Nikolic, S. Gao, G. Scarcelli, S. X. Sun, L. H. Romer and D. H. Gracias, *Adv. Sci.*, 2022, **9**, e2104649.
- 119 K. M. Schultz, K. A. Kyburz and K. S. Anseth, *Proc. Natl. Acad. Sci. U. S. A.*, 2015, **112**, E3757–E3764.
- 120 S. Kim, T. Kawai, D. Wang and Y. Yang, *ACS Appl. Mater. Interfaces*, 2016, **8**, 19245–19255.
- 121 X. Lu, Z. Ding, F. Xu, Q. Lu and D. L. Kaplan, *ACS Appl. Bio Mater.*, 2019, **2**, 3108–3119.



- 122 O. Chaudhuri, J. Cooper-White, P. A. Janmey, D. J. Mooney and V. B. Shenoy, *Nature*, 2020, **584**, 535–546.
- 123 Y. Zhao, S. Song, X. Ren, J. Zhang, Q. Lin and Y. Zhao, *Chem. Rev.*, 2022, **122**, 5604–5640.
- 124 C. T. Mierke, *Front. Cell Dev. Biol.*, 2022, **10**, 789841.
- 125 A. P. Dhand, J. H. Galarraga and J. A. Burdick, *Trends Biotechnol.*, 2021, **39**, 519–538.
- 126 G. Tansik and R. Stowers, *MRS Adv.*, 2024, **9**, 505–511.
- 127 M. Bernero, D. Zauchner, R. Müller and X.-H. Qin, *Biomater. Sci.*, 2024, **12**, 919–932.
- 128 P. Seth, J. Friedrichs, Y. D. P. Limasale, N. Fertala, U. Freudenberg, Y. Zhang, A. Lampel and C. Werner, *Adv. Healthc. Mater.*, 2025, **14**, e2402656.
- 129 M. Shayan, M. S. Huang, R. Navarro, G. Chiang, C. Hu, B. P. Oropeza, P. K. Johansson, R. A. Suhar, A. A. Foster, B. L. LeSavage, M. Zamani, A. Enejder, J. G. Roth, S. C. Heilshorn and N. F. Huang, *J. Biomed. Mater. Res., Part A*, 2023, **111**, 896–909.
- 130 M. Keshavarz and Q. Smith, *Adv. Funct. Mater.*, 2024, **34**, 2402360.
- 131 Z. Wei, R. Schnellmann, H. C. Pruitt and S. Gerecht, *Cell Stem Cell*, 2020, **27**, 798–812.
- 132 Z. Wei, M. Lei, Y. Wang, Y. Xie, X. Xie, D. Lan, Y. Jia, J. Liu, Y. Ma, B. Cheng, S. Gerecht and F. Xu, *Nat. Commun.*, 2023, **14**, 8307.
- 133 Q. Shen, R. R. Rigor, C. D. Pivetti, M. H. Wu and S. Y. Yuan, *Cardiovasc. Res.*, 2010, **87**, 272–280.
- 134 A. Totaro, T. Panciera and S. Piccolo, *Nat. Cell Biol.*, 2018, **20**, 888–899.
- 135 E. N. Olson and A. Nordheim, *Nat. Rev. Mol. Cell Biol.*, 2010, **11**, 353–365.
- 136 T. Azad, H. J. Janse van Rensburg, E. D. Lightbody, B. Neveu, A. Champagne, A. Ghaffari, V. R. Kay, Y. Hao, H. Shen, B. Yeung, B. A. Croy, K. L. Guan, F. Pouliot, J. Zhang, C. J. B. Nicol and X. Yang, *Nat. Commun.*, 2018, **9**, 1061.
- 137 G. E. Davis, A. N. Stratman, A. Sacharidou and W. Koh, *Int. Rev. Cell Mol. Biol.*, 2011, **288**, 101–165.
- 138 K. M. Wisdom, K. Adebawale, J. Chang, J. Y. Lee, S. Nam, R. Desai, N. S. Rossen, M. Rafat, R. B. West, L. Hodgson and O. Chaudhuri, *Nat. Commun.*, 2018, **9**, 4144.
- 139 D. Sun, K. Zhang, F. Zheng, G. Yang, M. Yang, Y. Xu, Y. Qin, M. Lin, Y. Li, J. Tan, Q. Li, X. Qu, G. Li, L. Bian and C. Zhu, *Adv. Mater.*, 2025, **37**, 2410802.
- 140 J. A. Beamish, B. A. Juliar, D. S. Cleveland, M. E. Busch, L. Nimmagadda and A. J. Putnam, *J. Biomed. Mater. Res., Part B*, 2019, **107**, 2507–2516.
- 141 L. Lin, R. E. Marchant, J. Zhu and K. Kottke-Marchant, *Acta Biomater.*, 2014, **10**, 5106–5115.
- 142 M. Vigen, J. Ceccarelli and A. J. Putnam, *Macromol. Biosci.*, 2014, **14**, 1368–1379.
- 143 L. Li, J. Yang, L. Perry, J. L. Bays, S. N. Bhatia, J. Eyckmans and C. S. Chen, *Commun. Biol.*, 2025, **8**, 1570.
- 144 X. Xiao, W. Wang, D. Liu, H. Zhang, P. Gao, L. Geng, Y. Yuan, J. Lu and Z. Wang, *Sci. Rep.*, 2015, **5**, 9409.
- 145 Y. C. Chiu, M. H. Cheng, H. Engel, S. W. Kao, J. C. Larson, S. Gupta and E. M. Brey, *Biomaterials*, 2011, **32**, 6045–6051.
- 146 W. Y. Wang, R. N. Kent 3rd, S. A. Huang, E. H. Jarman, E. H. Shikanov, C. D. Davidson, H. L. Hiraki, D. Lin, M. A. Wall, D. L. Matera, J. W. Shin, W. J. Polacheck, A. Shikanov and B. M. Baker, *Acta Biomater.*, 2021, **135**, 260–273.
- 147 K. Kick, K. Nekolla, M. Rehberg, A. M. Vollmar and S. Zahler, *Arterioscler., Thromb., Vasc. Biol.*, 2016, **36**, 2346–2357.
- 148 K. Wolf and P. Friedl, *Br. J. Dermatol.*, 2006, **154**(Suppl 1), 11–15.
- 149 F. Sabeh, R. Shimizu-Hirota and S. J. Weiss, *J. Cell Biol.*, 2009, **185**, 11–19.
- 150 N. Annabi, J. W. Nichol, X. Zhong, C. Ji, S. Koshy, A. Khademhosseini and F. Dehghani, *Tissue Eng. Part B. Rev.*, 2010, **16**, 371–383.
- 151 D. Lu, K. Cai, Z. Zeng, J. Huang, N. Ma, B. Gao and S. Yu, *Biomater. Adv.*, 2025, **167**, 214094.
- 152 Y. H. Cheng, S. J. Cheng, H. H. Chen and W. C. Hsu, *Colloids Surf., B*, 2022, **209**, 112150.
- 153 J. Visser, F. P. Melchels, J. E. Jeon, E. M. van Bussel, L. S. Kimpton, H. M. Byrne, W. J. Dhert, P. D. Dalton, D. W. Hutmacher and J. Malda, *Nat. Commun.*, 2015, **6**, 6933.
- 154 E. Rahimtoroghi, M. Kasra and H. Maleki, *Int. J. Polym. Mater. Polym. Biomater.*, 2022, **72**, 1294–1306.
- 155 D. Chen, B. Yang, C. Yang, J. Wu and Q. Zhao, *Chin. J. Chem.*, 2023, **41**, 3082–3096.
- 156 W. Dong, W. Ma, S. Zhao, X. Zhou, Y. Wang, Z. Liu, D. Sun, M. Zhang and Z. Jiang, *J. Mater. Chem. B*, 2022, **10**, 5473–5486.
- 157 C. Wang, L. Wang, Q. Zhang, L. Cheng, H. Yue, X. Xia and H. Zhou, *Colloids Surf., B*, 2021, **199**, 111441.
- 158 V. Samaryk, A. Voronov, I. Tarnavchyk, A. Kohut, N. Nosova, S. Varvarenko and S. Voronov, *J. Appl. Polym. Sci.*, 2009, **114**, 2204–2212.
- 159 J. S. Park, D. G. Woo, B. K. Sun, H. M. Chung, S. J. Im, Y. M. Choi, K. Park, K. M. Huh and K. H. Park, *J. Controlled Release*, 2007, **124**, 51–59.
- 160 K. D. Costa, E. J. Lee and J. W. Holmes, *Tissue Eng.*, 2003, **9**, 567–577.
- 161 J. A. Reid, K. D. Dwyer, P. R. Schmitt, A. H. Soepriatna, K. L. Coulombe and A. Callanan, *Biofabrication*, 2021, **13**, 045007.
- 162 S. Li, W. Yin, Y. Liu, C. Yang, Z. Zhai, M. Xie, Z. Ye and X. Song, *Biomater. Sci.*, 2025, **13**, 542–567.
- 163 A. Ray, O. Lee, Z. Win, R. M. Edwards, P. W. Alford, D. H. Kim and P. P. Provenzano, *Nat. Commun.*, 2017, **8**, 14923.
- 164 A. M. A. Suarez, I. van der Ham, M. G. L. Brinker, P. van Rijn and M. C. Harmsen, *Heliyon*, 2020, **6**, e04329.
- 165 Y. B. Li, M. Rukhlova, D. Zhang, J. Nhan, C. Sodja, E. Bedford, J. P. St-Pierre and A. Jezierski, *Tissue Eng. Part C. Methods*, 2024, **30**, 289–306.



- 166 F. Laco, M. H. Grant and R. A. Black, *J. Biomed. Mater. Res., Part A*, 2013, **101**, 1787–1799.
- 167 X. Li, B. Cho, R. Martin, M. Seu, C. Zhang, Z. Zhou, J. S. Choi, X. Jiang, L. Chen, G. Walia, J. Yan, M. Callanan, H. Liu, K. Colbert, J. Morrisette-McAlmon, W. Grayson, S. Reddy, J. M. Sacks and H. Q. Mao, *Sci. Transl. Med.*, 2019, **11**, eaau6210.
- 168 A. Ahmed, I. M. Joshi, M. Mansouri, N. N. N. Ahamed, M. C. Hsu, T. R. Gaborski and V. V. Abhyankar, *Am. J. Physiol. Cell Physiol.*, 2021, **320**, C1112–C1124.
- 169 E. S. Lai, N. F. Huang, J. P. Cooke and G. G. Fuller, *Regen. Med.*, 2012, **7**, 649–661.
- 170 M. G. McCoy, J. M. Wei, S. Choi, J. P. Goerger, W. Zipfel and C. Fischbach, *ACS Biomater. Sci. Eng.*, 2018, **4**, 2967–2976.
- 171 Y. L. Dorland and S. Huveneers, *Cell. Mol. Life Sci.*, 2017, **74**, 279–292.
- 172 H. Xu, H. Li, Q. Ke and J. Chang, *ACS Appl. Mater. Interfaces*, 2015, **7**, 8706–8718.
- 173 L. W. Dunne, T. Iyyanki, J. Hubenak and A. B. Mathur, *Acta Biomater.*, 2014, **10**, 3630–3640.
- 174 X. Li, P. Lu, Z. Liu, Z. Wen, X. Li, C. Wang, W. Jin, B. Zhou, N. Huang, M. Song and X. Wang, *Chem. Eng. J.*, 2023, **476**, 146745.
- 175 W. Guo, X. Wang, C. Yang, R. Huang, H. Wang and Y. Zhao, *Mater. Futures*, 2022, **1**, 015401.
- 176 X. Song, J. Zhang, S. Shen, D. Liu, J. Zhang, W. Yin, G. Ye, L. Wang, L. Cai, H. Hou and X. Qiu, *Research*, 2023, **6**, 0161.
- 177 Q. Liang, S. Chen, S. Hua, W. Jiang, J. Zhan, C. Pu, R. Lin, Y. He, H. Hou and X. Qiu, *Adv. Sci.*, 2025, **12**, e2400002.
- 178 Y. Jia, Z. Wei, J. Feng, M. Lei, Y. Yang, J. Liu, Y. Ma, W. Chen, G. Huang, G. M. Genin, X. Guo, Y. Li and F. Xu, *Research*, 2024, **7**, 0517.
- 179 A. Avendano, J. J. Chang, M. G. Cortes-Medina, A. J. Seibel, B. R. Admasu, C. M. Boutelle, A. R. Bushman, A. A. Garg, C. M. DeShetler, S. L. Cole and J. W. Song, *ACS Biomater. Sci. Eng.*, 2020, **6**, 1408–1417.
- 180 Y. D. Lin, C. Y. Luo, Y. N. Hu, M. L. Yeh, Y. C. Hsueh, M. Y. Chang, D. C. Tsai, J. N. Wang, M. J. Tang, E. I. Wei, M. L. Springer and P. C. Hsieh, *Sci. Transl. Med.*, 2012, **4**, 146ra109.
- 181 M. Salamone, S. Rigogliuso, A. Nicosia, S. Campora, C. M. Bruno and G. Ghersi, *Biomedicines*, 2021, **9**, 739.
- 182 A. N. Stratman, W. B. Saunders, A. Sacharidou, W. Koh, K. E. Fisher, D. C. Zawieja, M. J. Davis and G. E. Davis, *Blood*, 2009, **114**, 237–247.
- 183 K. R. Turner, C. Adams, S. Staelens, H. Deckmyn and J. San Antonio, *Anat. Rec.*, 2020, **303**, 1604–1618.
- 184 D. Baronas-Lowell, J. L. Lauer-Fields and G. B. Fields, *J. Biol. Chem.*, 2004, **279**, 952–962.
- 185 S. Abdalla, G. Makhoul, M. Duong, R. C. Chiu and R. Cecere, *Interact. Cardiovasc. Thorac. Surg.*, 2013, **17**, 767–772.
- 186 D. Baronas-Lowell, J. L. Lauer-Fields and G. B. Fields, *J. Biol. Chem.*, 2004, **279**, 952–962.
- 187 T. Furumatsu, N. Yamaguchi, K. Nishida, A. Kawai, T. Kunisada, M. Namba, H. Inoue and Y. Ninomiya, *J. Biochem.*, 2002, **131**, 619–626.
- 188 A. Sacharidou, W. Koh, A. N. Stratman, A. M. Mayo, K. E. Fisher and G. E. Davis, *Blood*, 2010, **115**, 5259–5269.
- 189 P. L. Chandran, D. C. Paik and J. W. Holmes, *Connect. Tissue Res.*, 2012, **53**, 285–297.
- 190 D. M. Casali, M. J. Yost and M. A. Matthews, *J. Biomed. Mater. Res., Part A*, 2018, **106**, 86–94.
- 191 K. Madhavan, D. Belchenko and W. Tan, *J. Biomed. Mater. Res., Part A*, 2011, **97**, 16–26.
- 192 H. G. Sundararaghavan, G. A. Monteiro, N. A. Lapin, Y. J. Chabal, J. R. Miksan and D. I. Shreiber, *J. Biomed. Mater. Res., Part A*, 2008, **87**, 308–320.
- 193 S. Ishihara, H. Kurosawa and H. Haga, *Gels*, 2023, **9**, 148.
- 194 J. M. Orban, L. B. Wilson, J. A. Kofroth, M. S. El-Kurdi, T. M. Maul and D. A. Vorp, *J. Biomed. Mater. Res., Part A*, 2004, **68**, 756–762.
- 195 C. Valero, H. Amaveda, M. Mora and J. M. Garcia-Aznar, *PLoS One*, 2018, **13**, e0195820.
- 196 C. O. Crosby, A. Hillsley, S. Kumar, B. Stern, S. H. Parekh, A. Rosales and J. Zoldan, *Acta Biomater.*, 2021, **122**, 133–144.
- 197 K. Sakaguchi, T. Shimizu, S. Horaguchi, H. Sekine, M. Yamato, M. Umezu and T. Okano, *Sci. Rep.*, 2013, **3**, 1316.
- 198 C. Liu, Y. Wu, H. Yang, K. Lu, H. Zhang, Y. Wang, J. Wang, L. Ruan, Z. Shen, Q. Yu and Y. Zhang, *J. Mater. Sci. Technol.*, 2023, **143**, 198–206.
- 199 A. J. Rufaihah, S. R. Vaibavi, M. Plotkin, J. Shen, V. Nithya, J. Wang, D. Seliktar and T. Kofidis, *Biomaterials*, 2013, **34**, 8195–8202.
- 200 T. P. Martens, A. F. Godier, J. J. Parks, L. Q. Wan, M. S. Koeckert, G. M. Eng, B. I. Hudson, W. Sherman and G. Vunjak-Novakovic, *Cell Transplant.*, 2009, **18**, 297–304.
- 201 F. S. Midekssa, C. D. Davidson, M. E. Wieger, J. L. Kamen, K. M. Hanna, D. K. P. Jayco, M. M. Hu, N. E. Friend, A. J. Putnam, A. S. Helms, A. Shikanov and B. M. Baker, *Bioact. Mater.*, 2025, **49**, 652–669.
- 202 A. Sahni, A. A. Khorana, R. B. Baggs, H. Peng and C. W. Francis, *Blood*, 2006, **107**, 126–131.
- 203 S. M. Anderson, S. N. Siegman and T. Segura, *Biomaterials*, 2011, **32**, 7432–7443.
- 204 A. Sahni and C. W. Francis, *Blood*, 2000, **96**, 3772–3778.
- 205 C. Radermacher, A. Rohde, V. Kucikas, E. M. Buhl, S. Wein, D. Jonigk, W. Jahnen-Dechent and S. Neuss, *Gels*, 2024, **10**, 820.
- 206 D. Whelan, N. M. Caplice and A. J. Clover, *J. Controlled Release*, 2014, **196**, 1–8.
- 207 T. A. Ahmed, M. Griffith and M. Hincke, *Tissue Eng.*, 2007, **13**, 1469–1477.
- 208 C. Williams, E. Budina, W. L. Stoppel, K. E. Sullivan, S. Emani, S. M. Emani and L. D. Black 3rd, *Acta Biomater.*, 2015, **14**, 84–95.
- 209 A. Petz, M. Grandoch, D. J. Gorski, M. Abrams, M. Piroth, R. Schneckmann, S. Homann, J. Muller, S. Hartwig,



- S. Lehr, Y. Yamaguchi, T. N. Wight, S. Gorressen, Z. Ding, S. Kotter, M. Kruger, A. Heinen, M. Kelm, A. Godecke, U. Flogel and J. W. Fischer, *Circ. Res.*, 2019, **124**, 1433–1447.
- 210 F. Bonafe, M. Govoni, E. Giordano, C. M. Caldarella, C. Guarnieri and C. Muscarelli, *J. Biomed. Sci.*, 2014, **21**, 100.
- 211 M. Salehi Namini, M. Khanmohammadi, N. Beheshtizadeh, M. S. Najafi, A. Heirani-Tabasi, A. Ayati, S. Boroumand, B. Pournemati, J. Ai, S. Ebrahimi-Barough, H. Montazerghaem and S. H. Ahmadi Tafti, *Int. J. Biol. Macromol.*, 2025, **304**, 140904.
- 212 A. G. Tavianatou, I. Caon, M. Franchi, Z. Piperigkou, D. Galesso and N. K. Karamanos, *FEBS J.*, 2019, **286**, 2883–2908.
- 213 S. Matou-Nasri, J. Gaffney, S. Kumar and M. Slevin, *Int. J. Oncol.*, 2009, **35**, 761–773.
- 214 F. Gao, C. X. Yang, W. Mo, Y. W. Liu and Y. Q. He, *Clin. Invest. Med.*, 2008, **31**, E106–E116.
- 215 M. V. Giraud, D. Di Francesco, M. C. Catoira, D. Cotella, L. Fusaro and F. Boccafroschi, *Biomedicines*, 2020, **8**, 436.
- 216 H. Tan, H. Li, J. P. Rubin and K. G. Marra, *J. Tissue Eng. Regen. Med.*, 2011, **5**, 790–797.
- 217 F. Lee, J. E. Chung and M. Kurisawa, *J. Controlled Release*, 2009, **134**, 186–193.
- 218 H. Li, B. Yu, P. Yang, J. Zhan, X. Fan, P. Chen, X. Liao, C. Ou, Y. Cai and M. Chen, *Biomaterials*, 2021, **279**, 121231.
- 219 L. Bian, C. Hou, E. Tous, R. Rai, R. L. Mauck and J. A. Burdick, *Biomaterials*, 2013, **34**, 413–421.
- 220 C. Wang, H. Hao, J. Wang, Y. Xue, J. Huang, K. Ren and J. Ji, *J. Mater. Chem. B*, 2021, **9**, 4024–4030.
- 221 R. L. Saunders and D. A. Hammer, *Cell. Mol. Bioeng.*, 2010, **3**, 60–67.
- 222 S. Bhutani, A. L. Y. Nachlas, M. E. Brown, T. Pete, C. T. Johnson, A. J. Garcia and M. E. Davis, *ACS Biomater. Sci. Eng.*, 2018, **4**, 200–210.
- 223 J. C. Huebsch, J. B. McCarthy, C. A. Diglio and D. L. Mooradian, *Circ. Res.*, 1995, **77**, 43–53.
- 224 G. Camci-Unal, J. W. Nichol, H. Bae, H. Tekin, J. Bischoff and A. Khademhosseini, *J. Tissue Eng. Regen. Med.*, 2013, **7**, 337–347.
- 225 T. Asakura, T. Hayashi, T. Tanaka, K. I. Tatematsu and H. Sezutsu, *J. Biomater. Appl.*, 2025, **40**, 402–418.
- 226 L. Kang, W. Jia, M. Li, Q. Wang, C. Wang, Y. Liu, X. Wang, L. Jin, J. Jiang, G. Gu and Z. Chen, *Carbohydr. Polym.*, 2019, **223**, 115106.
- 227 C. K. Perng, Y. J. Wang, C. H. Tsi and H. Ma, *J. Surg. Res.*, 2011, **168**, 9–15.
- 228 K. W. Lee, J. J. Yoon, J. H. Lee, S. Y. Kim, H. J. Jung, S. J. Kim, J. W. Joh, H. H. Lee, D. S. Lee and S. K. Lee, *Transplant Proc.*, 2004, **36**, 2464–2465.
- 229 S. Li, X. Wang, J. Chen, J. Guo, M. Yuan, G. Wan, C. Yan, W. Li, H. G. Machens, Y. Rinkevich, X. Yang, H. Song and Z. Chen, *Int. J. Biol. Macromol.*, 2022, **202**, 657–670.
- 230 M. Urbanova, M. Pavelkova, J. Czernek, K. Kubova, J. Vyslouzil, A. Pechova, D. Molinkova, J. Vyslouzil, D. Vetchy and J. Brus, *Biomacromolecules*, 2019, **20**, 4158–4170.
- 231 G. Kopplin, A. Lervik, K. I. Draget and F. L. Aachmann, *RSC Adv.*, 2021, **11**, 13780–13798.
- 232 J. Sun and H. Tan, *Materials*, 2013, **6**, 1285–1309.
- 233 I. Jain and N. F. Huang, *Arterioscler., Thromb., Vasc. Biol.*, 2024, **44**, A2062.
- 234 C. K. Kuo and P. X. Ma, *Biomaterials*, 2001, **22**, 511–521.
- 235 J. L. Drury, R. G. Dennis and D. J. Mooney, *Biomaterials*, 2004, **25**, 3187–3199.
- 236 Y. Feng, G. Kopplin, K. Sato, K. I. Draget and K. M. Varum, *Carbohydr. Polym.*, 2017, **156**, 490–497.
- 237 A. Liberski, N. Latif, C. Raynaud, C. Bollensdorff and M. Yacoub, *Glob. Cardiol. Sci. Pract.*, 2016, **2016**, e201604.
- 238 J. Leor, S. Tuvia, V. Guetta, F. Manczur, D. Castel, U. Willenz, O. Petnehazy, N. Landa, M. S. Feinberg, E. Konen, O. Goitein, O. Tsur-Gang, M. Shaul, L. Klapper and S. Cohen, *J. Am. Coll. Cardiol.*, 2009, **54**, 1014–1023.
- 239 J. M. Singelyn and K. L. Christman, *Macromol. Biosci.*, 2011, **11**, 731–738.
- 240 J. L. Ungerleider, T. D. Johnson, N. Rao and K. L. Christman, *Methods*, 2015, **84**, 53–59.
- 241 D. Bejleri and M. E. Davis, *Adv. Healthc. Mater.*, 2019, **8**, e1801217.
- 242 J. A. Claudio-Rizo, M. Rangel-Argote, L. E. Castellano, J. Delgado, J. L. Mata-Mata and B. Mendoza-Novelo, *Mater. Sci. Eng., C*, 2017, **79**, 793–801.
- 243 S. B. Seif-Naraghi, D. Horn, P. J. Schup-Magoffin and K. L. Christman, *Acta Biomater.*, 2012, **8**, 3695–3703.
- 244 Y. Seo, Y. Jung and S. H. Kim, *Acta Biomater.*, 2018, **67**, 270–281.
- 245 E. Vorotnikova, D. McIntosh, A. Dewilde, J. Zhang, J. E. Reing, L. Zhang, K. Cordero, K. Bedelbaeva, D. Gourevitch, E. Heber-Katz, S. F. Badylak and S. J. Braunhut, *Matrix Biol.*, 2010, **29**, 690–700.
- 246 J. W. Wassenaar, R. Gaetani, J. J. Garcia, R. L. Braden, C. G. Luo, D. Huang, A. N. DeMaria, J. H. Omens and K. L. Christman, *J. Am. Coll. Cardiol.*, 2016, **67**, 1074–1086.
- 247 J. M. Singelyn, J. A. DeQuach, S. B. Seif-Naraghi, R. B. Littlefield, P. J. Schup-Magoffin and K. L. Christman, *Biomaterials*, 2009, **30**, 5409–5416.
- 248 P. Kong, J. Dong, W. Li, Z. Li, R. Gao, X. Liu, J. Wang, Q. Su, B. Wen, W. Ouyang, S. Wang, F. Zhang, S. Feng, D. Zhuang, Y. Xie, G. Zhao, H. Yi, Z. Feng, W. Wang and X. Pan, *Adv. Sci.*, 2023, **10**, e2301244.
- 249 R. M. Wang and K. L. Christman, *Adv. Drug Delivery Rev.*, 2016, **96**, 77–82.
- 250 G. N. Grover, N. Rao and K. L. Christman, *Nanotechnology*, 2014, **25**, 014011.
- 251 G. Papavasiliou, S. Sokic, M. Turturro, G. Papavasiliou, S. Sokic and M. Turturro, *Biotechnology – Molecular Studies and Novel Applications for Improved Quality of Human Life*, IntechOpen, 2012.
- 252 J. J. Moon, M. S. Hahn, I. Kim, B. A. Nsiah and J. L. West, *Tissue Eng., Part A*, 2009, **15**, 579–585.



- 253 M. V. Turturro, S. Sokic, J. C. Larson and G. Papavasiliou, *Biomed. Mater.*, 2013, **8**, 025001.
- 254 E. A. Phelps, N. O. Enemchukwu, V. F. Fiore, J. C. Sy, N. Murthy, T. A. Sulchek, T. H. Barker and A. J. Garcia, *Adv. Mater.*, 2012, **24**, 64–70.
- 255 M. H. Ghanian, H. Mirzadeh and H. Baharvand, *Eco-friendly and Smart Polymer Systems*, 2020.
- 256 J. Yu, F. Chen, X. Wang, N. Dong, C. Lu, G. Yang and Z. Chen, *Polym. Degrad. Stab.*, 2016, **133**, 312–320.
- 257 K. A. Gunay, T. L. Ceccato, J. S. Silver, K. L. Bannister, O. J. Bednarski, L. A. Leinwand and K. S. Anseth, *Angew. Chem., Int. Ed.*, 2019, **58**, 9912–9916.
- 258 A. Samourides, L. Browning, V. Hearnden and B. Chen, *Mater. Sci. Eng., C*, 2020, **108**, 110384.
- 259 G. P. Raeber, M. P. Lutolf and J. A. Hubbell, *Biophys. J.*, 2005, **89**, 1374–1388.
- 260 A. Navaei, D. Truong, J. Heffernan, J. Cutts, D. Brafman, R. W. Sirianni, B. Vernon and M. Nikkhah, *Acta Biomater.*, 2016, **32**, 10–23.
- 261 K. L. Fujimoto, Z. Ma, D. M. Nelson, R. Hashizume, J. Guan, K. Tobita and W. R. Wagner, *Biomaterials*, 2009, **30**, 4357–4368.
- 262 S. Firoozi, S. Pahlavan, M.-H. Ghanian, S. Rabbani, S. Tavakol, M. Barekat, S. Yakhkeshi, E. Mahmoudi, M. Soleymani and H. Baharvand, *Biomolecules*, 2020, **10**, 205.
- 263 Z. Li and J. Guan, *Polymers*, 2011, **3**, 740–761.
- 264 G. Camci-Unal, N. Annabi, M. R. Dokmeci, R. Liao and A. Khademhosseini, *NPG Asia Mater.*, 2014, **6**, e99.
- 265 B. Pena, M. Laughter, S. Jett, T. J. Rowland, M. R. G. Taylor, L. Mestroni and D. Park, *Macromol. Biosci.*, 2018, **18**, e1800079.
- 266 C. B. Raub, A. J. Putnam, B. J. Tromberg and S. C. George, *Acta Biomater.*, 2010, **6**, 4657–4665.
- 267 S. O. Sarrigiannidis, J. M. Rey, O. Dobre, C. Gonzalez-Garcia, M. J. Dalby and M. Salmeron-Sanchez, *Mater. Today Bio*, 2021, **10**, 100098.
- 268 H. Duong, B. Wu and B. Tawil, *Tissue Eng., Part A*, 2009, **15**, 1865–1876.
- 269 W. M. Gramlich, I. L. Kim and J. A. Burdick, *Biomaterials*, 2013, **34**, 9803–9811.
- 270 Y. W. Ding, Z. Y. Wang, Z. W. Ren, X. W. Zhang and D. X. Wei, *Biomater. Sci.*, 2022, **10**, 3393–3409.
- 271 S. S. Soofi, J. A. Last, S. J. Liliensiek, P. F. Nealey and C. J. Murphy, *J. Struct. Biol.*, 2009, **167**, 216–219.
- 272 K. M. Mabry, R. L. Lawrence and K. S. Anseth, *Biomaterials*, 2015, **49**, 47–56.
- 273 S. P. Singh, M. P. Schwartz, J. Y. Lee, B. D. Fairbanks and K. S. Anseth, *Biomater. Sci.*, 2014, **2**, 1024–1034.
- 274 I. Jorba, M. Nikolic and C. V. C. Bouten, in *Cardiac Mechanobiology in Physiology and Disease*, ed. M. Hecker and D. J. Duncker, Springer International Publishing, Cham, 2023, ch. 8, pp. 181–210, DOI: [10.1007/978-3-031-23965-6\\_8](https://doi.org/10.1007/978-3-031-23965-6_8).
- 275 R. Ebrahimihaei, N. Tarassova, S. C. Bond, M. C. McNeill, T. Hathway, H. Vohra, A. C. Newby and M. Bond, *Biochim. Biophys. Acta. Mol. Cell Res.*, 2024, **1871**, 119640.
- 276 F. Shahabipour, N. Ashammakhi, R. K. Oskuee, S. Bonakdar, T. Hoffman, M. A. Shokrgozar and A. Khademhosseini, *Transl. Res.*, 2020, **216**, 57–76.
- 277 U. Sarig, E. B. Nguyen, Y. Wang, S. Ting, T. Bronshtein, H. Sarig, N. Dahan, M. Gvirtz, S. Reuveny, S. K. Oh, T. Scheper, Y. C. Boey, S. S. Venkatraman and M. Machluf, *Tissue Eng., Part A*, 2015, **21**, 1507–1519.
- 278 S. Shafiee, S. Shariatzadeh, A. Zafari, A. Majd and H. Niknejad, *Front. Bioeng. Biotechnol.*, 2021, **9**, 745314.
- 279 Z. Ataie, S. Horchler, A. Jaber, S. V. Koduru, J. C. El-Mallah, M. Sun, S. Kheirabadi, A. Kedzierski, A. Risbud, A. Silva, D. J. Ravnic and A. Sheikhi, *Small*, 2024, **20**, e2307928.
- 280 H. Li, K. S. Iyer, L. Bao, J. Zhai and J. J. Li, *Adv. Healthc. Mater.*, 2024, **13**, e2301597.
- 281 S. Hom, J. O'Hara, W. Yin and D. Rubenstein, *FASEB J.*, 2015, **29**, 792.
- 282 J. J. Kim, L. Hou, G. Yang, N. P. Mezak, M. Wanjare, L. M. Joubert and N. F. Huang, *Cell. Mol. Bioeng.*, 2017, **10**, 417–432.
- 283 N. E. Friend, A. Y. Rioja, Y. P. Kong, J. A. Beamish, X. Hong, J. C. Habif, J. R. Bezenah, C. X. Deng, J. P. Stegemann and A. J. Putnam, *Sci. Rep.*, 2020, **10**, 15562.
- 284 X. Sun, J. Wu, B. Qiang, R. Romagnuolo, M. Gagliardi, G. Keller, M. A. Laflamme, R. K. Li and S. S. Nunes, *Sci. Transl. Med.*, 2020, **12**, eaax2992.
- 285 T. Dvir, A. Kedem, E. Ruvinov, O. Levy, I. Freeman, N. Landa, R. Holbova, M. S. Feinberg, S. Dror, Y. Etzion, J. Leor and S. Cohen, *Proc. Natl. Acad. Sci. U. S. A.*, 2009, **106**, 14990–14995.
- 286 M. A. Redd, N. Zeinstra, W. Qin, W. Wei, A. Martinson, Y. Wang, R. K. Wang, C. E. Murry and Y. Zheng, *Nat. Commun.*, 2019, **10**, 584.
- 287 M. B. Esch, D. J. Post, M. L. Shuler and T. Stokol, *Tissue Eng., Part A*, 2011, **17**, 2965–2971.
- 288 A. Herland, A. D. van der Meer, E. A. FitzGerald, T.-E. Park, J. J. F. Sleeboom and D. E. Ingber, *PLoS One*, 2016, **11**, e0150360.
- 289 R. Booth, S. Noh and H. Kim, *Lab Chip*, 2014, **14**, 1880–1890.
- 290 M. Lindner, A. Laporte, L. Elomaa, C. Lee-Thedieck, R. Olmer and M. Weinhart, *Front. Cell Dev. Biol.*, 2022, **10**, 953062.
- 291 M. Floryan, E. Cambria, A. Blazeski, M. F. Coughlin, Z. Wan, G. Offeddu, V. Vinayak, A. Kant, J. Whisler, V. Shenoy and R. D. Kamm, *npj Biol. Phys. Mech.*, 2025, **2**, 24.
- 292 Y. Wu, J. Fu, Y. Huang, R. Duan, W. Zhang, C. Wang, S. Wang, X. Hu, H. Zhao, L. Wang, J. Liu, G. Gao and P. Yuan, *Animal Model. Exp. Med.*, 2023, **6**, 337–345.
- 293 J. Gonzalez-Rubio, H. Kubiza, Y. Xu, H. Koenigs-Werner, M. S. Schmitz, M. Schedel, C. Apel, S. Jockenhoevel,



- C. G. Cornelissen and A. L. Thiebes, *Adv. Sci.*, 2025, **12**, e2408131.
- 294 T. Mathur, K. A. Singh, N. K. R. Pandian, S.-H. Tsai, T. W. Hein, A. K. Gaharwar, J. M. Flanagan and A. Jain, *Lab Chip*, 2019, **19**, 2500–2511.
- 295 H. J. Weener, T. F. van Haaps, R. W. J. van Helden, H. J. Albers, R. Haverkate, H. H. T. Middelkamp, M. L. Ridderikhof, T. E. van Mens, A. van den Berg, C. L. Mummery, V. V. Orlova, S. Middeldorp, N. van Es and A. D. van der Meer, *Lab Chip*, 2025, **25**, 1787–1800.
- 296 Y. C. Chen, R. Z. Lin, H. Qi, Y. Yang, H. Bae, J. M. Melero-Martin and A. Khademhosseini, *Adv. Funct. Mater.*, 2012, **22**, 2027–2039.
- 297 C. H. Lin, J. J. Su, S. Y. Lee and Y. M. Lin, *J. Tissue Eng. Regen. Med.*, 2018, **12**, 2099–2111.
- 298 Y. A. Geiger, B. K. Kaufmann, B. E. Hartmann, M. Rudolph, E. R. Borrero, A. Silva, O. Hayden, H. Clausen-Schaumann and S. Sudhop, *Bioprinting*, 2025, **52**, e00455.
- 299 C. Shen, Y. Li, Y. Wang and Q. Meng, *Lab Chip*, 2019, **19**, 3962–3973.
- 300 E. Y. Wang, N. Rafatian, Y. Zhao, A. Lee, B. F. L. Lai, R. X. Lu, D. Jekic, L. Davenport Huyer, E. J. Knee-Walden, S. Bhattacharya, P. H. Backx and M. Radisic, *ACS Cent. Sci.*, 2019, **5**, 1146–1158.
- 301 M. A. Skylar-Scott, S. G. M. Uzel, L. L. Nam, J. H. Ahrens, R. L. Truby, S. Damaraju and J. A. Lewis, *Sci. Adv.*, 2019, **5**, eaaw2459.
- 302 M. Rahimnejad, A. Adoungotchodo, N. R. Demarquette and S. Lerouge, *Bioprinting*, 2022, **27**, e00209.
- 303 F. Afghah, M. Altunbek, C. Dikyol and B. Koc, *Sci. Rep.*, 2020, **10**, 5257.
- 304 K. C. Cheng, P. Theato and S. H. Hsu, *Biofabrication*, 2023, **15**, 045026.
- 305 I. W. Zhang, L. S. Choi, N. E. Friend, A. J. McCoy, F. S. Midekssa, M. M. Hu, E. Alsberg, S. C. Leshner-Pérez, J. P. Stegemann, B. M. Baker and A. J. Putnam, *Acta Biomater.*, 2025, **201**, 283–296.
- 306 B. Grigoryan, S. J. Paulsen, D. C. Corbett, D. W. Sazer, C. L. Fortin, A. J. Zaita, P. T. Greenfield, N. J. Calafat, J. P. Gounley, A. H. Ta, F. Johansson, A. Randles, J. E. Rosenkrantz, J. D. Louis-Rosenberg, P. A. Galie, K. R. Stevens and J. S. Miller, *Science*, 2019, **364**, 458–464.
- 307 Z. Wang, R. Abdulla, B. Parker, R. Samanipour, S. Ghosh and K. Kim, *Biofabrication*, 2015, **7**, 045009.
- 308 S. James and T. Shivakumar, *Preliminary Study on Effects of the Process Parameters on Mechanical Properties in Liquid Holographic Volumetric Additive Manufacturing Process*, 2019.
- 309 J. Madrid-Wolff, A. Boniface, D. Loterie, P. Delrot and C. Moser, *Adv. Sci.*, 2022, **9**, e2105144.
- 310 X. Han, J. Courseaus, J. Khamassi, N. Nottrodt, S. Engelhardt, F. Jacobsen, C. Bierwisch, W. Meyer, T. Walter, J. Weisser, R. Jaeger, R. Bibb and R. Harris, *Int. J. Bioprint.*, 2018, **4**, 134.
- 311 C. Wang and Y. Zhou, *Manuf. Lett.*, 2024, **41**, 375–383.
- 312 G. Dong, Q. Lian, L. Yang, W. Mao, S. Liu and C. Xu, *J. Bionic Eng.*, 2018, **15**, 673–681.
- 313 S. Maharjan, J. J. He, L. Lv, D. Wang and Y. S. Zhang, in *Vascular Tissue Engineering: Methods and Protocols*, ed. F. Zhao and K. W. Leong, Springer US, New York, NY, 2022, pp. 61–75, DOI: [10.1007/978-1-0716-1708-3\\_6](https://doi.org/10.1007/978-1-0716-1708-3_6).
- 314 Q. Pi, S. Maharjan, X. Yan, X. Liu, B. Singh, A. M. van Genderen, F. Robledo-Padilla, R. Parra-Saldivar, N. Hu, W. Jia, C. Xu, J. Kang, S. Hassan, H. Cheng, X. Hou, A. Khademhosseini and Y. S. Zhang, *Adv. Mater.*, 2018, **30**, e1706913.
- 315 X. Zhou, M. Nowicki, H. Sun, S. Y. Hann, H. Cui, T. Esworthy, J. D. Lee, M. Plesniak and L. G. Zhang, *ACS Appl. Mater. Interfaces*, 2020, **12**, 45904–45915.
- 316 S. Wang, J. Li, Z. Ma, L. Sun, L. Hou, Y. Huang, Y. Zhang, B. Guo and F. Yang, *Front. Bioeng. Biotechnol.*, 2021, **9**, 794769.
- 317 X. Wang, X. Li, Y. Zhang, X. Long, H. Zhang, T. Xu and C. Niu, *Front. Bioeng. Biotechnol.*, 2021, **9**, 761861.
- 318 F. Shahabipour, M. Tavafoghi, G. E. Aninwene II, S. Bonakdar, R. K. Oskuee, M. A. Shokrgozar, T. Potyondy, F. Alambeigi and S. Ahadian, *J. Biomed. Mater. Res., Part A*, 2022, **110**, 1077–1089.
- 319 J. S. Miller, K. R. Stevens, M. T. Yang, B. M. Baker, D. H. Nguyen, D. M. Cohen, E. Toro, A. A. Chen, P. A. Galie, X. Yu, R. Chaturvedi, S. N. Bhatia and C. S. Chen, *Nat. Mater.*, 2012, **11**, 768–774.
- 320 Q. Gao, Y. He, J. Z. Fu, A. Liu and L. Ma, *Biomaterials*, 2015, **61**, 203–215.
- 321 Q. Liang, F. Gao, Z. Zeng, J. Yang, M. Wu, C. Gao, D. Cheng, H. Pan, W. Liu and C. Ruan, *Adv. Funct. Mater.*, 2020, **30**, 2001485.
- 322 N. de Paiva Narciso, R. S. Navarro, A. E. Gilchrist, M. L. M. Trigo, G. Aviles Rodriguez and S. C. Heilshorn, *Adv. Healthc. Mater.*, 2023, **12**, e2301265.
- 323 C. E. Vorwald, T. Gonzalez-Fernandez, S. Joshee, P. Sikorski and J. K. Leach, *Acta Biomater.*, 2020, **108**, 142–152.
- 324 S. V. Rao, U. Zeymer, P.S. Douglas, H. Al-Khalidi, J. A. White, J. Liu, H. Levy, V. Guetta, C. M. Gibson, J.-F. Tanguay, P. Vermeersch, J. Roncalli, J. D. Kasprzak, T. D. Henry, N. Frey, O. Kracoff, J. H. Traverse, P. Chew Derek, J. Lopez-Sendon, R. Heyrman and M. W. Krucoff, *JACC*, 2016, **68**, 715–723.
- 325 K. Elvitigala, W. Mubarak and S. Sakai, *Polymers*, 2022, **14**, 5034.

